ELSEVIER

NeuroImage

www.elsevier.com/locate/ynimg
NeuroImage 24 (2005) 398–416

Program for Assisted Labeling of Sulcal Regions (PALS): description and reliability

Maryam E. Rettmann,[a,b,*] Duygu Tosun,[c] Xiaodong Tao,[c] Susan M. Resnick,[a] and Jerry L. Prince[c]

[a]National Institute on Aging, National Institutes of Health, Baltimore, MD 21224, USA
[b]Department of Biomedical Engineering, Johns Hopkins University, Baltimore, MD 21218, USA
[c]Department of Electrical and Computer Engineering, Johns Hopkins University, Baltimore, MD 21218, USA

Received 9 April 2004; revised 29 July 2004; accepted 4 August 2004

With the improvements in techniques for generating surface models from magnetic resonance (MR) images, it has recently become feasible to study the morphological characteristics of the human brain cortex in vivo. Studies of the entire surface are important for measuring global features, but analysis of specific cortical regions of interest provides a more detailed understanding of structure. We have previously developed a method for automatically segmenting regions of interest from the cortical surface using a watershed transform. Each segmented region corresponds to a cortical sulcus and is thus termed a "sulcal region." In this work, we describe two important augmentations of this methodology. First, we describe a user interface that allows for the efficient labeling of the segmented sulcal regions called the Program for Assisted Labeling of Sulcal Regions (PALS). An additional augmentation allows for even finer divisions on the cortex with a methodology that employs the fast marching technique to track a curve on the cortical surface that is then used to separate segmented regions. After regions of interest have been identified, we compute both the cortical surface area and gray matter volume. Reliability experiments are performed to assess both the long-term stability and short-term repeatability of the proposed techniques. These experiments indicate the proposed methodology gives both highly stable and repeatable results.

Keywords: Human brain cortex; Watershed; Fast marching; Cortical features; Sulci; Sulcus

Introduction

With the improvements in techniques for generating surface models from Magnetic Resonance (MR) images, there has recently been increased interest in the quantitative morphometric analysis of the human cerebral cortical surface and its sulci (Cachia et al., 2003a; Crespo-Facorro et al., 1999; Davatzikos and Bryan, 2002; Fischl and Dale, 2000; Grenander and Miller, 1998; Kim et al., 2000; Le Goualher et al., 1999; Magnotta et al., 1999; Manceaux-Demiau et al., 1998; Miller et al., 2000; Ratnanather et al., 2001, 2003; Thompson et al., 1996a,b, 2000; Toga and Thompson, 2002; Toga et al., 2001; Vaillant and Davatzikos, 1997; Van Essen and Drury, 1997; Zeng et al., 1999; Zhou et al., 1999). In addition to global analyses, there has also been interest in analyzing specific regional morphological characteristics of the cortical surface. One of the major challenges in regional analysis is in the definition of regions of interest on the cortical surface. As gyri and sulci have traditionally been used for defining location on the cortical surface, several groups have used these anatomical structures to delineate regions of interest (cf. Cachia et al., 2003b; Caviness et al., 1996; Crespo-Facorro et al., 1999; Fischl et al., 2004; Jouandet et al., 1989; Kim et al., 2000; Rademacher et al., 1992; Tzourio et al., 1997).

We have also used this general philosophy for defining regions of interest on the cortex and have previously described a methodology for segmenting "sulcal regions" from a cortical surface (Rettmann et al., 2002b). We define "sulcal regions" as the buried cortical regions surrounding the sulcal spaces as illustrated in a simplified cross-section in Fig. 1 and similar in concept to the "sulcal basins" proposed in Lohmann and von Cramon (2000). In this work, we describe two important augmentations of this methodology. First, we describe a user interface that allows for the efficient manual labeling of the segmented sulcal regions that is facilitated by a graph-based structure of the cortical sulci. Several other groups (Le Goualher et al., 1999; Mangin et al., 1995a,b, 2003; Royackkers et al., 1999) have also utilized graph-based representations of the cortical sulci with a variety of approaches and applications. Second, we describe a semiautomated technique, which, if necessary, can be utilized to further divide the segmented regions. This technique employs the fast marching algorithm (Kimmel and Sethian, 1998) to track a curve on the cortical surface, which is then used to separate segmented regions.

* Corresponding author. Cognition Section, Laboratory of Personality and Cognition, National Institute on Aging, 5600 Nathan Shock Drive, Baltimore, MD 21224. Fax: +1 410 558 8674.
E-mail addresses: maryam.rettmann@nih.gov (M.E. Rettmann), dtosun@jhu.edu (D. Tosun), xtao2@jhu.edu (X. Tao), susan.resnick@nih.gov (S.M. Resnick), prince@jhu.edu (J.L. Prince).
Available online on ScienceDirect (www.sciencedirect.com).

1053-8119/$ - see front matter © 2004 Elsevier Inc. All rights reserved.
doi:10.1016/j.neuroimage.2004.08.014

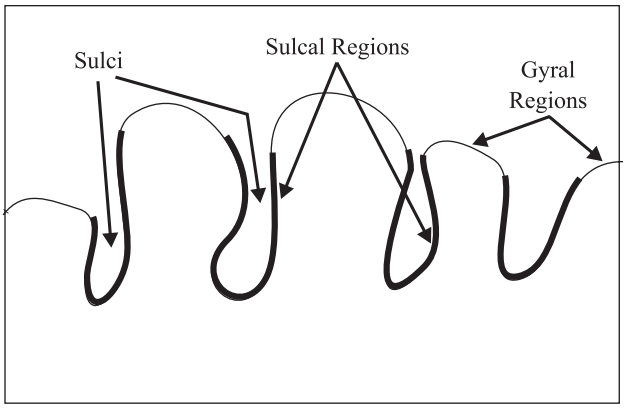

Fig. 1. Simplified cross-section of a cortical surface illustrating "sulcal regions".

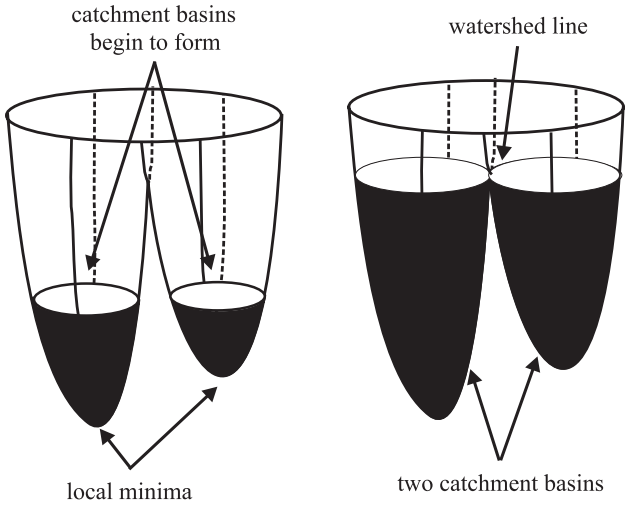

Fig. 3. An illustration of the watershed transform.

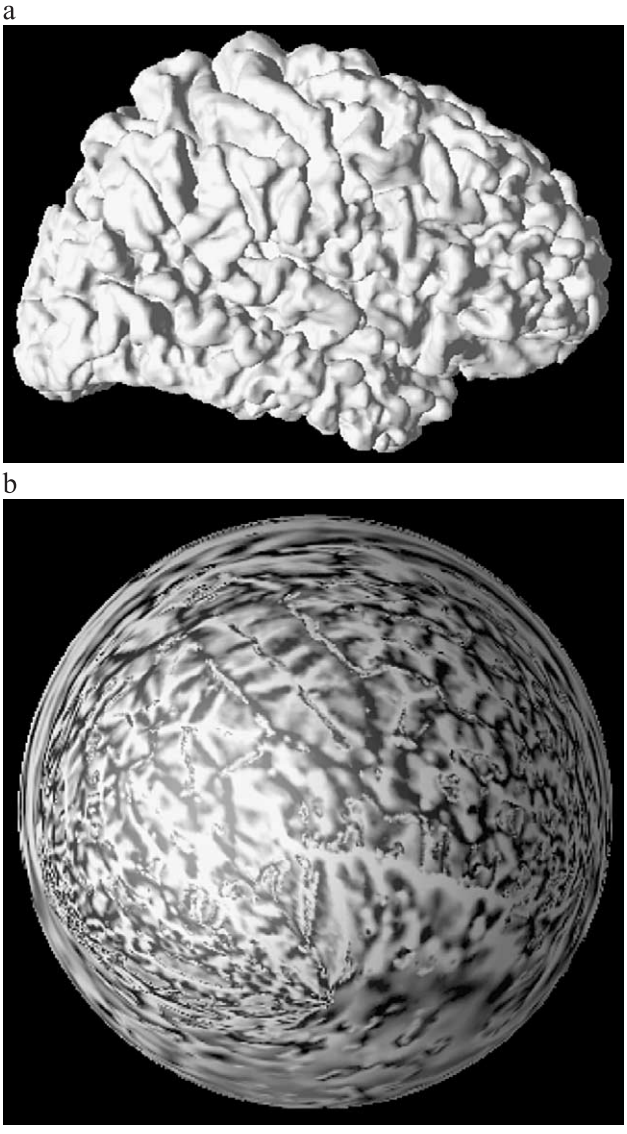

Fig. 2. (a) A reconstructed cortical surface and (b) its corresponding spherical map with mean curvature displayed.

We believe the proposed semiautomatic methodology is preferable to a purely manual approach—for example, manually tracing sulcal regions on the cortical surface. First, a purely manual tracing approach would be extremely laborious and time consuming. Second, the boundaries of the sulcal region could not be defined as consistently. In our approach, the sulcal boundaries are consistently defined using an automated algorithm. Third, it would be extremely difficult to utilize the full three-dimensional geometric information of the cortical structure if tracing along the outer (visible) cortex. Our approach can separate regions based on ridges hidden deep within the cortical folds because it utilizes the geometry of the entire cortical sheet (including the buried regions) during the segmentation procedure.

The morphometric characterization of the cortical surface has gained increased interest in recent years. Studies are beginning to indicate differences in cortical thickness, volume, and shape as well as variations in sulcal patterns associated with specific diseases (Cannon et al., 2002; Chan et al., 2003; Kikinis et al., 1994; Kuperberg et al., 2003; Leonard et al., 1993; Levitt et al., 2003; Miller et al., 2003; Molko et al., 2003; Raz et al., 1995; Rosas et al., 2002; Sailer et al., 2003; Scahill et al., 2002; Sebire et al., 1995; Thompson et al., 1998, 2001a,b, 2003). There is also evidence of cortical changes in both normal and diseased aging (Good et al., 2001; Magnotta et al., 1999; Murphy et al., 1996;

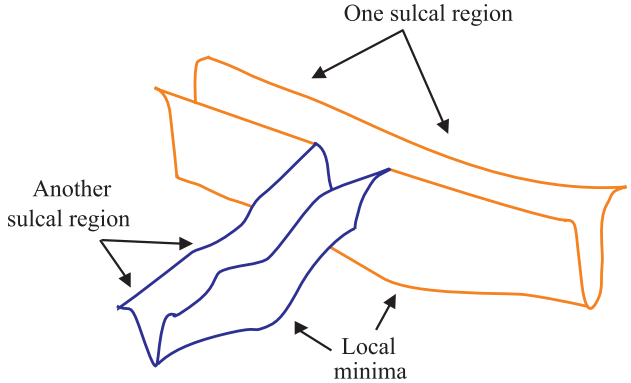

Fig. 4. An illustration of how the watershed transform can be used to segment sulcal regions.

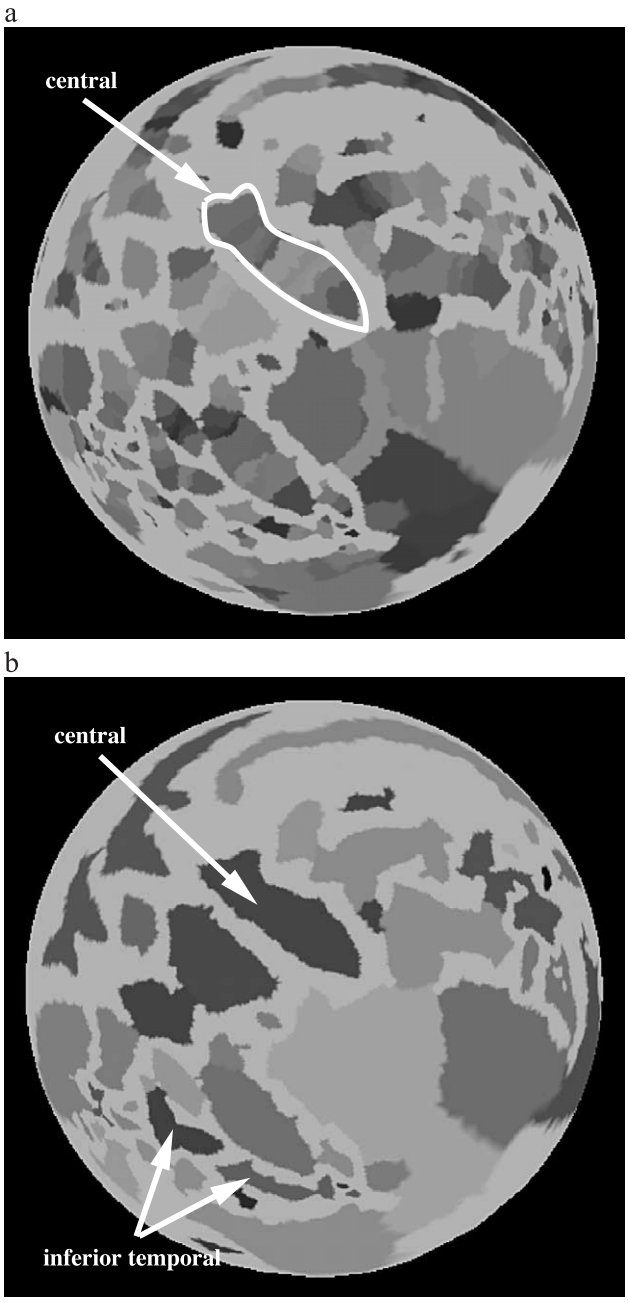

Fig. 5. (a) Catchment basins identified by the watershed transform on the cortical surface and (b) merged catchment basins providing a segmentation of sulcal regions.

Pfefferbaum et al., 1994; Raz et al., 1997; Resnick et al., 2000, 2003; Salat et al., 2004; Scahill et al., 2003; Sowell et al., 2003; Sullivan et al., 1995). In any study of cortical morphometrics, it is critical that both the segmentation of regions of interest as well as measurements of these regions are highly repeatable. In the case of a longitudinal study, it is also important that measurements are stable across data sets acquired over many years. In this work, we conduct reliability studies that assess both the long-term stability as well as the short-term repeatability of the proposed techniques. The long-term stability analysis is conducted on a set of 35 subjects scanned over a 4-year interval and assesses the correlation of regional measurements across this time span. The short-term repeatability is a "test–retest" analysis on three individuals who were each scanned twice within a 30-min time interval. These experiments indicate the techniques and measurements are both highly stable and repeatable. We note that a preliminary version of this work has been previously published as a conference paper (Rettmann et al., 2002a).

Background

All MR imaging data used in this work were obtained from the Baltimore Longitudinal Study of Aging (Resnick et al., 2000; Shock et al., 1984). We use the basic approach that has been previously described (Xu et al., 1999) to find a cortical surface from a volumetric MR image. The method combines fuzzy segmentation, isosurfaces, and deformable surface models to reconstruct a surface lying at the geometric center of the cortex. Techniques reported in Han et al. (2001a,b) and Xu et al. (2000) were used to improve upon the original methodology. A reconstructed cortical surface is represented by a triangular mesh consisting of approximately 300,000 vertices, as shown in Fig. 2a.

To permit visualization of the entire cortical surface—including the buried cortical folds—we generate a spherical

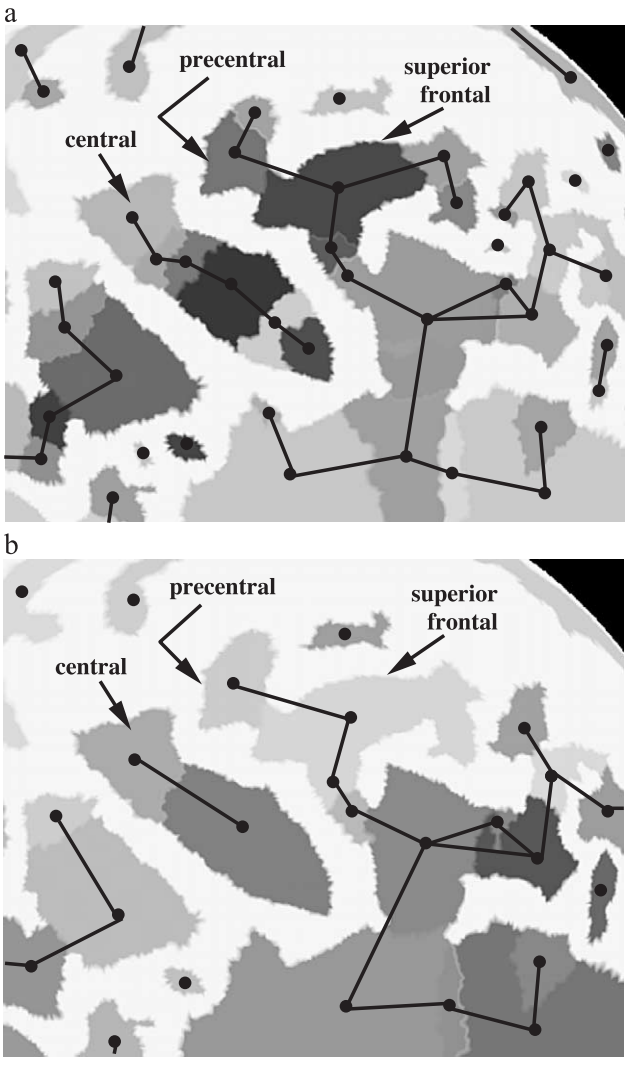

Fig. 6. Catchment basins are represented by graphs at different "levels" of merging.

representation for each hemisphere of the reconstructed cortical surface (Tosun and Prince, 2001). This representation has a one-to-one mapping with the original reconstructed surface and makes visualization of the entire cortical surface easy. For example, the mean curvature of the cortical surface in Fig. 2a is shown on its spherical map in Fig. 2b.

Given a reconstructed cortical surface, we segment the sulcal regions using a watershed segmentation technique (Rettmann et al., 2002b). As the data representations used in this technique are important in the present application, we give an overview of the approach. First, the hemispheres are separated so the medial sulcal regions are also segmented. Next, the geodesic depth is computed for each vertex on the triangle mesh that lies within a sulcal region using the fast marching technique (Kimmel and Sethian, 1998). The geodesic depth is defined as the length of the shortest path, along the surface, from each point within a sulcal region to the "outer cortex". We use geodesic distance rather than three-dimensional Euclidean distance as a measure of depth because it is a natural measure on the surface itself. We define "outer cortex" as that part of the cortex that is visible without opening up the cortical folds. A watershed transform (cf. Meyer and Beucher, 1990; Vincent and Soille, 1991) is then computed on the triangle mesh using a "height function" defined as the maximum geodesic depth minus the actual geodesic depth.

The watershed transform determines *catchment basins* on the cortical surface, the concept of which can be understood by studying Fig. 3. As depicted on the left, the watershed transform can be viewed as puncturing holes in the local minima of a height function followed by an immersion of this function into a pool of water. When the water from two regions begins to merge, a watershed line is constructed, which prevents water in one region from spilling into the other. When the immersion is complete, each of the regions associated with a minimum forms a separate catchment basin.

The concept of how the watershed transform can be used to segment cortical sulcal regions is illustrated in Fig. 4. This geometric structure represents a possible configuration of two sulcal regions. In this figure, there are two local minima, each associated with a sulcal region. If a watershed transform is applied to this geometric structure, two catchment basins will form—one associated with each local minimum. Each catchment basin, shown in orange and blue, corresponds to a distinct sulcal region. This figure specifically illustrates how the watershed can distinguish sulcal regions separated by a "buried" ridge (i.e., one that is hidden within the sulcal folds).

Catchment basins produced by the watershed transform applied to a cortical surface are shown in Fig. 5a on a spherical map. We note that all processing is done on the *original* cortical surface—the spherical map is used for visualization purposes only. It is clear from Fig. 5a that single sulcal regions are often represented by several catchment basins. For example, the region of cortex corresponding to the central sulcus consists of approximately 10 catchment basins in Fig. 5a. This kind of "oversegmentation" is a typical result of the watershed algorithm (Vincent and Soille, 1991). To address this problem, we developed a merging algorithm that combines catchment basins to better define the sulcal regions (Rettmann et al., 2002b). Our general criteria for merging is that sulcal regions should be separated by either gyral regions on the outer cortex or by large ridges at the watershed lines, and that

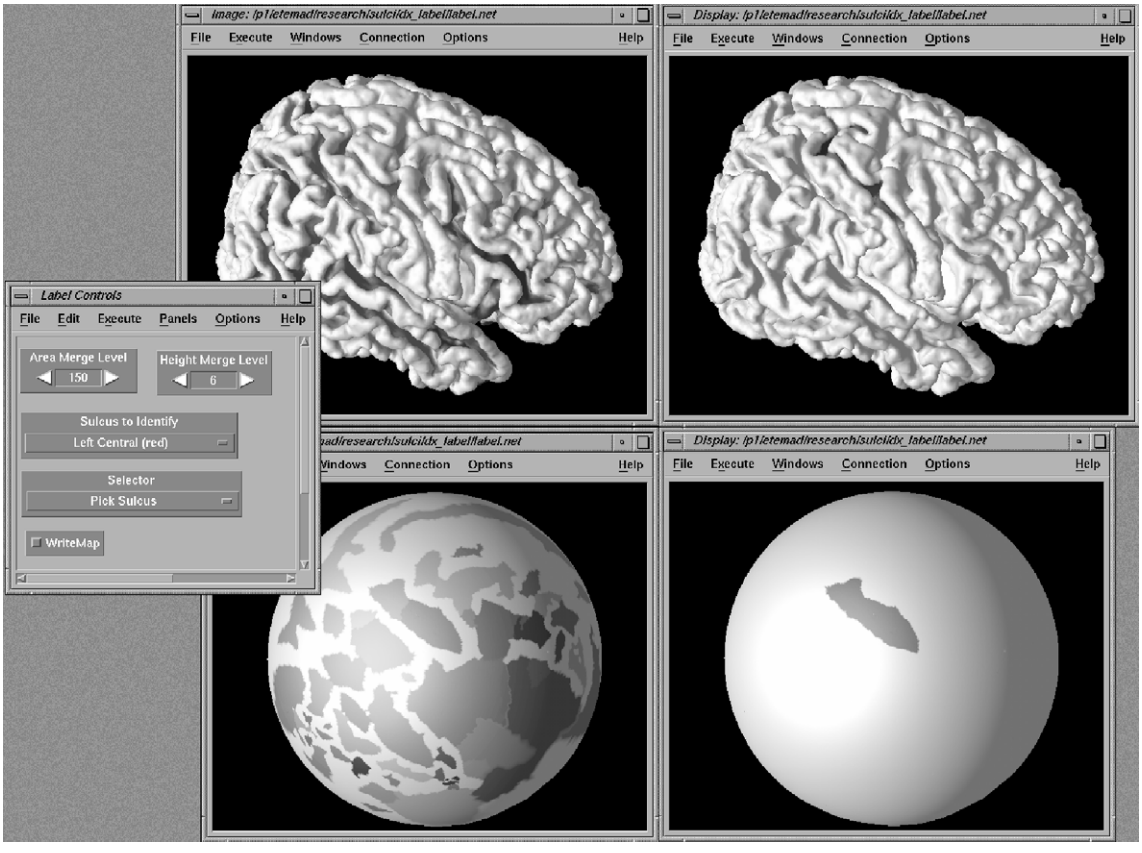

Fig. 7. Program for Assisted Labeling of Sulcal Regions (PALS).

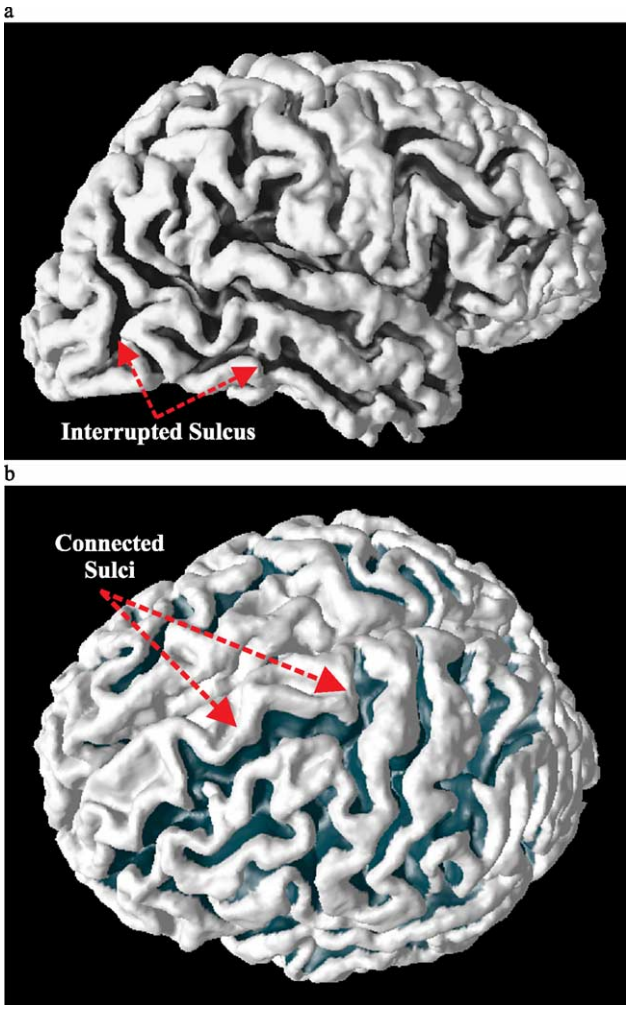

Fig. 8. Example of interrupted and connected sulci.

sulcal regions are generally large. Accordingly, we developed two criteria for the merging algorithm. First, if the height of the ridge separating two catchment basins is smaller than a designated threshold, then the two catchment basins are merged. Second, if the area of a catchment basin is less than a designated threshold, it is merged with the largest adjacent catchment basin. The resulting sulcal segmentation, which combines the watershed transform and catchment basin merging, is shown in Fig. 5b. We see from this figure that the sulcal region corresponding to the central sulcus now consists of just one piece. This figure also demonstrates that in the case of interrupted sulci (sulci that are interrupted by a gyral ridge Ono et al., 1990), the sulcal region will still exist as several pieces. In this example, the inferior temporal sulcus is interrupted, and is thus segmented as two pieces even after the merging algorithm.

Methods

Labeling techniques

In this section, we describe a system for efficiently assigning labels to the segmented sulcal regions. An additional augmentation is also described which allows for even finer division of regions on the cortex. The watershed algorithm previously described is generally very good at identifying the correct sulcal regions; however, it is not perfect. Occasionally, the algorithm will combine catchment basins that should not be combined. For labeling purposes, we must be able to "undo" this merge, and separately label the catchment basins. It is also common for sulci to be interrupted or pseudo-interrupted (Ono et al., 1990). These types of sulci are broken into more than one piece by a gyral ridge and are thus segmented in multiple pieces according to our definition of sulcal regions. In this case, multiple pieces must be grouped together to form a single sulcal region of interest.

Sometimes, sulcal regions are *not* separated by any ridge, so a single catchment basin crosses sulcal regions that must be given different names. Separating individual catchment basins into separate regions is facilitated by an algorithm that calculates geodesics on the triangle mesh and splits the single region into two

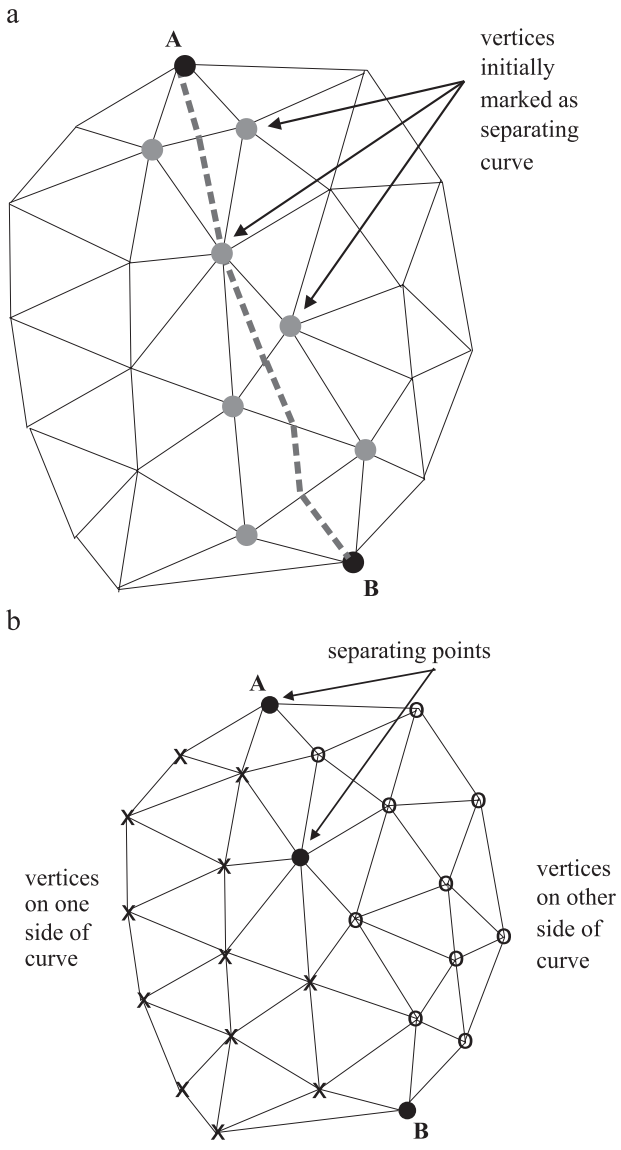

Fig. 9. (a) Vertices initially marked as belonging to the separating curve and (b) result of region separation where ×'s indicate vertices on one side of the curve and ○'s indicate vertices on the other side of the curve.

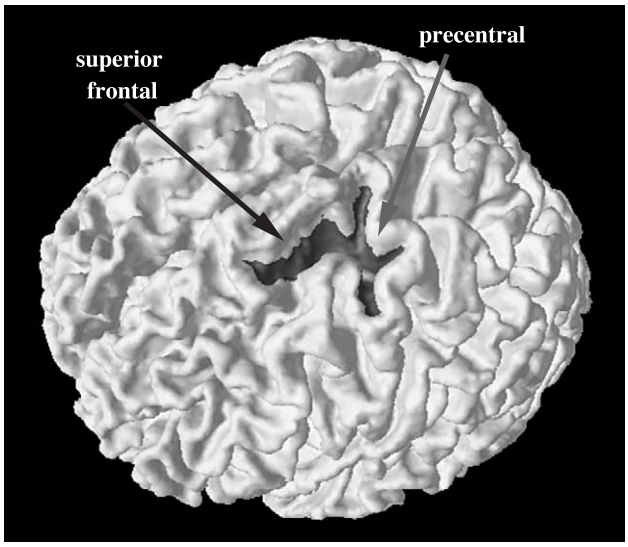

Fig. 10. Superior frontal and precentral sulci are segmented as one piece (illustrated at a higher level of merging).

regions lying on either side of the geodesic curve. The geodesic curve is the shortest length path between two points that lies on the surface.

All of these capabilities are combined together into a user interface called the Program for Assisted Labeling of Sulcal Regions (PALS), which makes it easy for a user to label regions of interest on the cortical surface. In this section, we describe this user interface and the algorithms that provide the capabilities described above.

Program for Assisted Labeling of Sulcal Regions (PALS)

The purpose of PALS is to provide the ability to efficiently label sulcal regions of interest. To this end, it is most desirable to do this labeling after the catchment basins have been appropriately merged in the sulcal segmentation algorithm. In the merging step, catchment basins are merged based on two criteria—the height of the ridge separating two catchment basins and the area of a catchment basin. Clearly, different values of these parameters will lead to different "levels" or amounts of merging. As both the "ridge height" and "area" thresholds increase, more merging takes place. In general, we would like to label sulcal regions at the level where all the catchment basins corresponding to a single sulcal region have been merged. However, due to the complex nature of the cortical folds, it is generally impossible to identify a single set of parameters that will work equally well across the entire cortical surface. Thus, we use a hierarchical merging approach where various "levels" of the merging algorithm are computed and stored.

The hierarchical merging is organized by first building an adjacency graph of the catchment basins. Each catchment basin is considered to be a node on the graph and links between the nodes indicate that catchment basins are adjacent to one other—i.e., they share a boundary. For example, part of the graph structure around the central sulcal region is shown in Fig. 6a at a lower level of merging (i.e., less merging). The graph structure of the same region at a higher level of merging (i.e., more merging) is shown in Fig. 6b. As one moves between levels, regions merge and separate, thus providing a rich data structure where the optimal level can quickly be determined for each region of interest.

The user interface PALS, illustrated in Fig. 7, provides this capability [implemented using OpenDX (OpenDX Developers, http://www.opendx.org/, Based on IBM's Visualization Data Explorer)]. The interface has two basic displays, each consisting of both a cortical surface and a spherical map. The first display (seen on the left in Fig. 7) has the catchment basins superimposed on the spherical map and cortical surface at the level selected by the user. The user can select the ridge height and area merging levels using a control bar. The user selects a sulcus to label using a drop-down menu and selects the appropriate regions by clicking on either surface—cortex or sphere—using a mouse. We generally found it easiest to visually identify sulci on the cortex and subsequently select the region on the spherical map. The selected regions are then colored on the "labeled" surfaces (shown on the right) with a predesignated color for each sulcus. This allows for

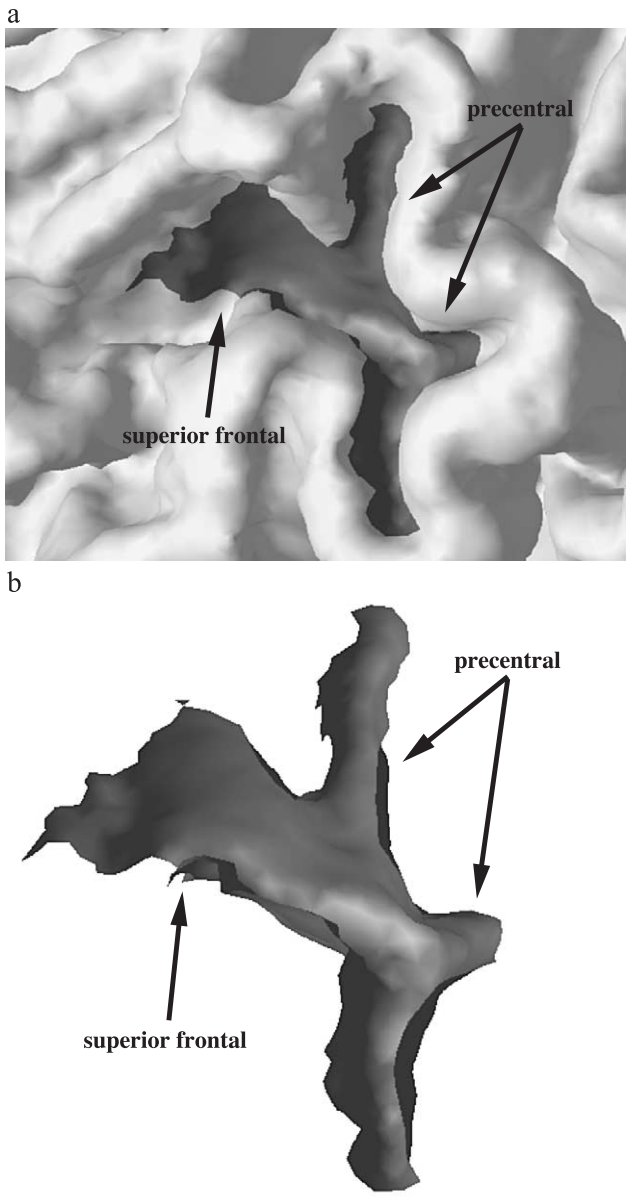

Fig. 11. (a) Superior frontal and precentral sulci at lowest merging level (i.e., no merging) and (b) a zoomed up view of this catchment basin.

the efficient labeling of sulcal regions. For example, the central sulcus can typically be selected at a "high" level of merging—i.e., a single click can label many catchment basins, which significantly

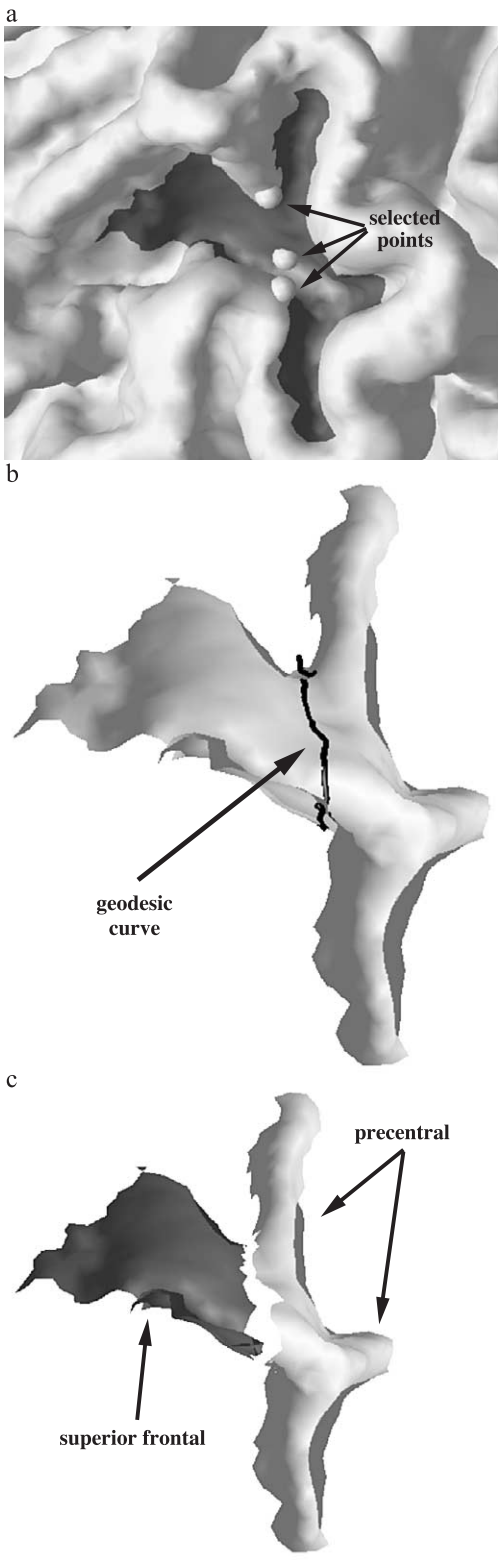

Fig. 12. (a) Three points selected for curve tracking algorithm; (b) curve generated from tracking algorithm for splitting catchment basin into two pieces; and (c) catchment basin split into two pieces.

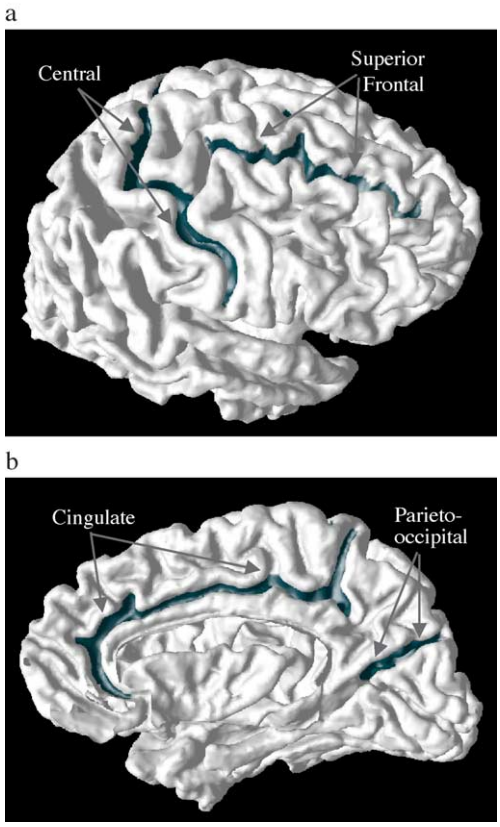

Fig. 13. The locations of the sulcal regions labeled on (a) the lateral surface and (b) the medial surface.

reduces overall labeling time. The interface has the ability to label sulcal regions on all cortical surfaces—i.e., the lateral, medial, and inferior.

There are certain cortical sulci that are often interrupted or pseudo-interrupted (Ono et al., 1990). These types of sulci consist of two or more pieces separated by a gyral ridge. Interrupted sulci are separated by a gyral ridge that is visible on the outer cortical surface, while pseudo-interrupted sulci are separated by gyral ridges buried within the sulcal folds (Ono et al., 1990). In the case of interrupted sulci, the watershed with merging algorithm will segment the multiple pieces of the sulcal region separately as they are divided by a gyral ridge. In the case of pseudo-interrupted sulci, the multiple pieces will be joined only if the height of the ridge separating the adjacent pieces is less than the ridge height threshold. Sulci are actually interrupted quite frequently. For example, in an analysis of 25 brains, the inferior temporal sulcus was interrupted 96% of the time on the right and 100% of the time on the left (Ono et al., 1990). An example of an interrupted inferior temporal sulcal region is shown in Fig. 8a. In this case, the inferior temporal sulcus consists of two separate pieces. Whether a sulcal region is truly interrupted or pseudo-interrupted, there is potentially the need to group various segmented regions together to be labeled as a single sulcal region—a capability provided by PALS. The user simply chooses the name of the sulcus from the drop-down menu and then selects all the pieces associated with that sulcal region with the mouse.

These two features of PALS allow for the labeling of the majority of sulcal regions. However, there are certain sulci that are often "connected" (Ono et al., 1990), meaning there is no ridge

separating them. For example, the precentral and superior frontal sulci are often connected as illustrated in Fig. 8b. The watershed generates separate basins based on ridges on the cortical surface. Thus, in the case of connected sulci, the watershed cannot properly separate these sulcal regions and another methodology must be employed. The basic idea for the catchment basin separation is to first generate a curve that separates the region and then use this curve in conjunction with a region growing technique to separate the region.

Curve tracking

In this section, we review how to construct geodesic curves on a triangulated mesh utilizing a technique called "Fast Marching" (see also Bartesaghi and Sapiro, 2001 for a more detailed description). The Fast Marching method is a numerical approach for solving Eikonal equations (Kimmel and Sethian, 1998):

$$|\nabla T(\vec{x})| f(\vec{x}) = 1, \quad \vec{x} \in \mathcal{C}, \tag{1}$$

where $\mathcal{C}$ is a manifold, T is the arrival time of a wavefront propagating on the manifold and $f(\vec{x})$ is the speed at a particular point, $\vec{x}$. The key idea is to simulate a wave propagating from an initial position on a surface. The wave propagates through each node with a speed defined on that node. The speed can be uniform on the entire surface, in which case the arrival time of the wave is equivalent to geodesic distance, or different from node to node, making the arrival time of the wave dependent on the speed of the nodes through which it has traveled. This method can be used to construct curves along the surface in the following manner. First, the two end points of the curve, A and B, are selected on the surface. Next, the Eikonal equation is solved with boundary condition $T(A) = 0$ (and the speed term set appropriately). Finally, a curve is constructed by backtracking the gradient direction of T from B (Kimmel and Sethian, 1998).

Region division

A segmented cortical region can be separated by using a curve that traverses through the region in conjunction with a region growing technique. The goal is to create two regions—one on each side of the curve. This is accomplished by assigning each vertex a label indicating which of the two regions it lies in. In the implementation of the tracking program used in this work (Tao et al., 2001), an extracted 3-D curve is expressed by an ordered list of points on the surface containing either vertices or locations on the edges through which the curve traverses. All vertices through which the curve traverses are marked as belonging to the separating curve. In addition, the two vertices associated with an edge through which the curve traverses are also marked as belonging to the separating curve as illustrated in Fig. 9a. Next, vertices on one side of the curve are found using a region growing technique beginning at a seed point (selected manually) on that side of the curve. The separating curve points provide a boundary for the region growing. The same procedure is subsequently performed on the other side. As a final step, vertices labeled as lying along the separating curve because they were associated with an edge are relabeled using the labels assigned to their neighboring (noncurve) vertices as illustrated in Fig. 9b.

Catchment basin separation

As previously mentioned, the watershed transform cannot always separate two sulcal regions, i.e., in the case where there is no ridge separating them. One area of the brain where this is prone to occur is at the junction between the superior frontal and precentral sulci (Ono et al., 1990). An example of this is shown in Fig. 10 where the black region on the cortex corresponds to the automatically segmented region at a higher level of merging. Normally, when labeling these two regions, the user would move through lower levels of merging until these two regions split. However, as shown in Fig. 11a, even at the lowest level of merging (i.e., no merging), these regions are still connected. This occurs because no ridge exists between these sulci as seen in Fig. 11b. This region can, however, be split by generating a "separating curve" and using this in conjunction with the region division algorithm. The separating curve is generated using the previously described geodesic curve tracking algorithm along with points manually selected by the user. These points indicate where the curve should pass on the surface and are selected using mouse clicks on the cortical surface. Suppose, for example, a user selects four points through which the curve should pass—call them points A, B, C, and D. The curve is then tracked as follows: first, the geodesic curve from point D to point C is computed; next, the geodesic curve from point C to point B is computed; and, finally, the geodesic curve from point B to point A is computed. The final separating curve is a concatenation of each of these individual curves. In this example, the points selected for the curve generation are shown in Fig. 12a (the points are enlarged for visualization purposes) and the resulting curve is shown in Fig. 12b. Seed points were selected for the regions

Table 1
Types of operations required for labeling each of the sulcal regions

Type of operation	Ce_l	Ce_r	SF_l	SF_r	$Cing_l$	$Cing_r$	PO_l	PO_r
One piece at default level	73	87	20	38	8	26	70	81
One piece at default level + removed pieces at lower level	5	6	5	8	10	17	12	7
One piece at default level + added pieces at lower level	4	0	14	5	4	1	0	0
One piece at default level + removed and added pieces at lower level	0	0	2	5	2	0	0	0
One piece at lower level	0	0	0	0	1	1	0	0
Grouped pieces at default level	6	10	36	37	33	23	16	15
Grouped pieces at default level + removed pieces at lower level	0	1	9	7	20	13	2	1
Grouped pieces at default level + added pieces at lower level	1	0	4	0	1	2	2	0
Grouped pieces at default level + removed and added pieces at lower level	0	0	5	0	2	0	0	0
Grouped pieces at lower level	15	0	8	4	23	20	1	0
Catchment basin separations	4	0	134	136	3	1	99	97

During the labeling procedure, we found the surface model generated for one data set at one time point appeared noisy and inaccurate and was therefore dropped from the analysis. In addition, of the 832 sulcal regions labeled, three were not segmented correctly and were also dropped from the analysis.

on either side of the curve and the final separated regions are shown in Fig. 12c. After the region separation, "separating points" (see Fig. 9) are not assigned to either region (and thus their associated triangles are not assigned to either region). For certain calculations (i.e., surface area), these triangles will need to be appropriately divided between the regions as addressed in the next section. We note that while we call this procedure a "catchment basin separation", the same technique can be used to separate any segmented region (i.e., a collection of catchment basins that have been grouped together at a higher merging level). We use the term "catchment basin separation" to describe any of these separations for ease of terminology in subsequent sections.

Region measurements

Surface area

For each of the segmented and labeled sulcal regions, we compute two measurements—surface area and gray matter volume. The first measure, surface area, quantifies the cortical surface area of a sulcal region. For sulcal regions that are labeled without the requirement of a catchment basin separation, the area computation is straightforward. Area is computed as the sum of the areas of the triangles that lie within the labeled region. The area computation for sulcal regions that require the separation of a catchment basin requires additional consideration. Referring back to Fig. 9a, we see there are two types of triangles, those that lie completely on one side of the curve and those that are divided by the separating curve. In the first case, the entire area of the triangle is added to its corresponding region. In the second case, the area of the triangle needs to be appropriately divided between the two regions. A triangle is divided by creating temporary points on the edges where the curve passes through—in effect dividing the triangle into either two smaller triangles or a triangle and a four-sided polygon. These areas are then computed and added to the appropriate regions.

Gray matter volume

The gray matter volume is a measure of the amount of cortical gray matter corresponding to each sulcal region and is computed using both surface area and cortical thickness. We use the method described in Han et al. (2001c) to compute cortical thickness. In this approach, cortical thickness is computed from the image volume using distance transforms from the gray matter/white matter and gray matter/cerebrospinal fluid interfaces. A thickness value is assigned to each grid point in the volume that lies between the two interfaces and is defined as the sum of the distances from the point to each of the two interfaces. The reconstructed cortical surface is generated in the same coordinate space as the image volume, which means that each vertex can obtain image values by directly mapping into the image data in the volume. Accordingly, we obtain measures of cortical thickness at each vertex using trilinear interpolation applied in the image volume containing estimates of cortical thickness at volumetric grid points.

For sulcal regions that are labeled without the requirement of a catchment basin separation, the volume is computed as the sum of the volumes of the individual triangles that lie within the labeled region. The volume of each triangle is computed as the product of its area and the thickness at the center of the triangle. The volume computation for sulcal regions that require the separation of a catchment basin require a similar procedure as that described in the surface area calculation. As described previously, triangles divided by the separating curve are divided into either two triangles or a triangle and a four-sided polygon. In this case, these individual volumes are computed as the product of the surface area and the thickness at the center of either the triangle or the polygon and subsequently added to the appropriate regions.

Reliability assessment

The first reliability experiment assesses the long-term stability of the area and gray matter volume measurements. The data used in

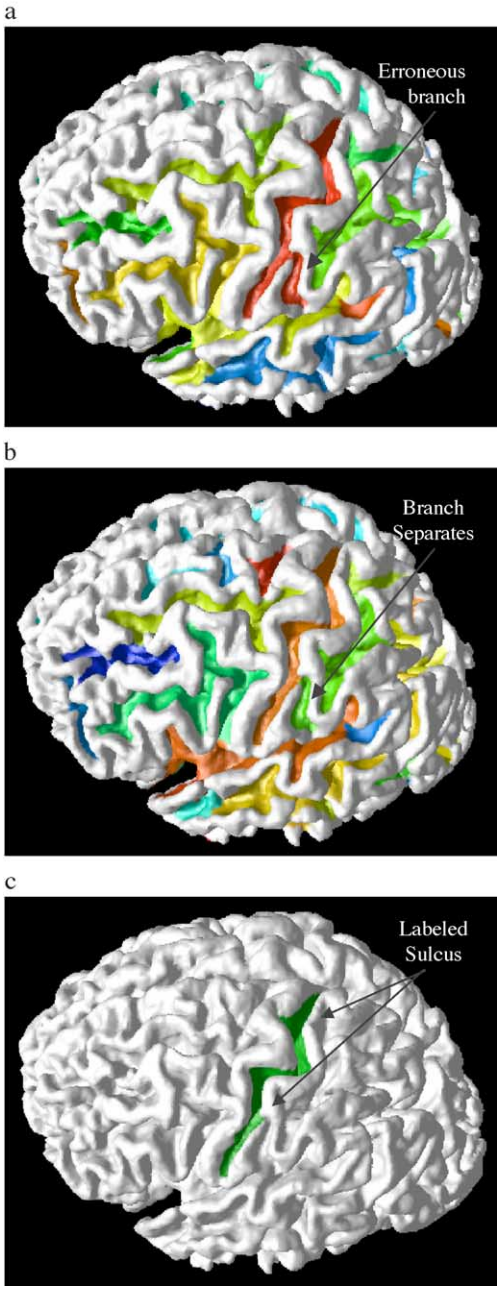

Fig. 14. At the default merging level, there is a connection between the central sulcal region and a branch over the postcentral gyrus (a). This branch is disconnected by lowering the merging level as illustrated in b, allowing the user to properly label the central sulcal region as shown in c.

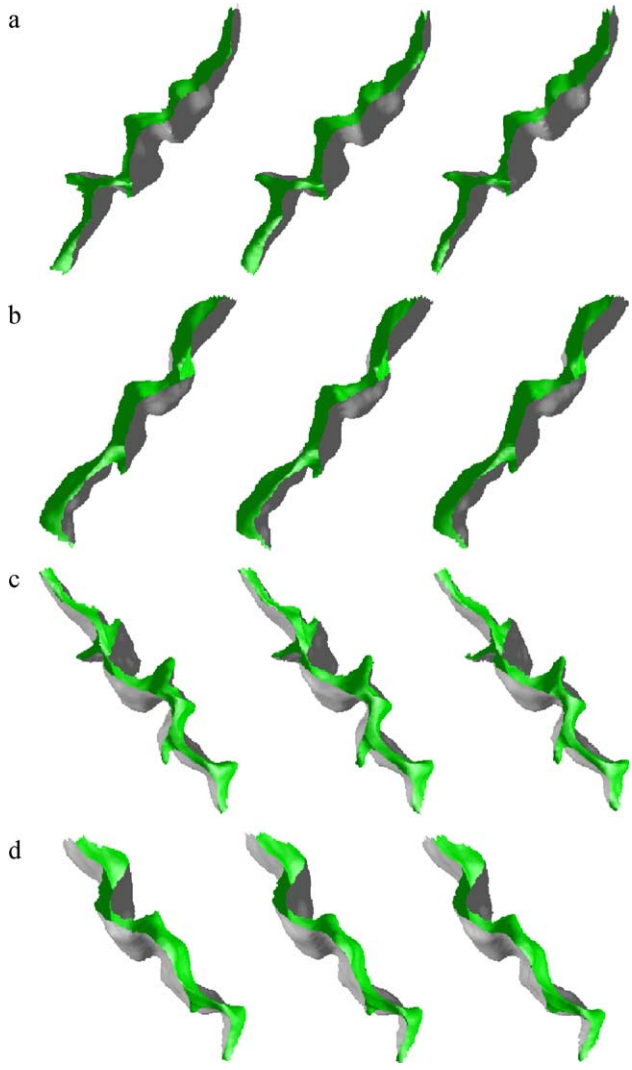

Fig. 15. The labeled left (a, b) and right (c, d) central sulcal regions for the three scans of various individuals.

this analysis is a set of longitudinal data in which 35 individuals were each scanned three times over a 4-year time period. Thus, we have three data sets from each of 35 individuals. In this analysis, a substantial amount of time has passed between the scans and it is conceivable that the underlying anatomy has actually changed during this time period. Therefore, in this analysis, the area and volume measurements computed from multiple scans will reflect both long-term stability of the measures as well as anatomic change. For this reason, we do not necessarily expect that the measures from year to year will be exactly the same; however, we do expect a high correlation between the repeated measurements (i.e., a measurement from one scan should be able to predict the measurement of a repeated scan albeit higher or lower).

The second reliability experiment is a repeatability analysis that assesses the short-term "test–retest" repeatability of our methods. The data for this analysis consists of three individuals who were each scanned twice within a 30-min time interval. Between each scan, the individuals were repositioned within the scanner. Thus, we have two data sets from each of three individuals that represent the same underlying anatomy. The goal of this analysis was to use these data sets to determine the short-term repeatability of the

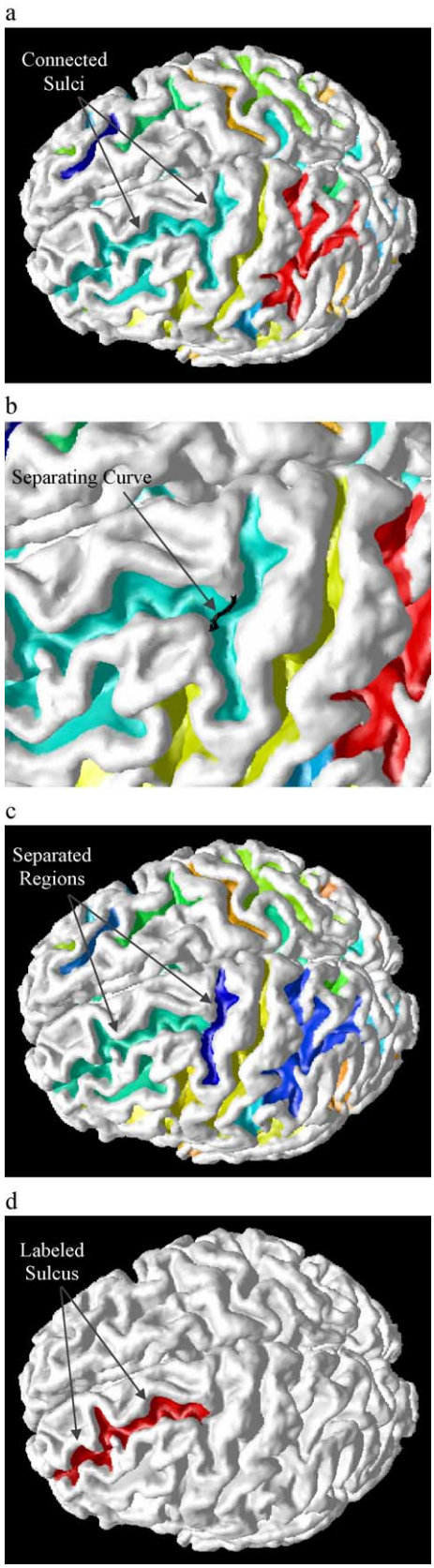

Fig. 16. At the default merging level, the superior frontal and precentral sulcal regions are connected (a). The catchment basin separation operation is used to separate these regions with the separating curve shown in b and the separated regions shown in c. The final labeled region is illustrated in d.

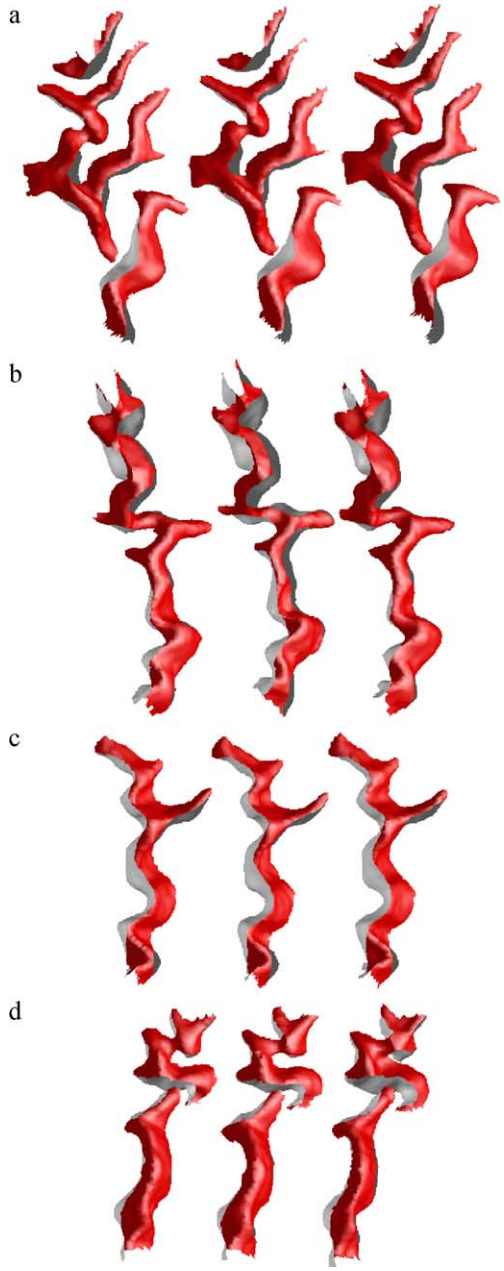

Fig. 17. The labeled left (a, b) and right (c, d) superior frontal sulcal regions for the three scans of various individuals.

entire procedure from the image acquisition through all image-processing steps. Starting with the data from each pair of scans, we compute the cortical surface models and sulcal segmentations as well as the area and gray matter volume measurements. If the entire procedure is error-free, we would obtain identical results for each pair of data sets.

Sources of error

There are several potential sources of error that are reflected in the short-term repeatability measure. The first is the image acquisition itself. Factors such as RF inhomogeneities in the MR scanner and patient motion can lead to variations in the images acquired. Next, the surface reconstruction technique will produce different results on the two data sets. The magnitude of this difference depends on how robust the reconstruction technique is to the image variations. The next potential source of error is in the sulcal segmentation and labeling procedure. This error depends on how robust the sulcal segmentation is to small variations in the cortical surface and how consistently a user can assign anatomic labels to the surface pairs. We now explain each of the reliability experiments in more detail.

Stability analysis

In the stability analysis, 35 individuals were each scanned three times over a 4-year interval providing a scan at year 1, year 3, and year 5. Before transferring the data sets from the BLSA database, the data set names were encoded such that the year of acquisition for each scan was unknown. Next, the cortical reconstructions, sulcal segmentations, and spherical maps were generated for all 105 data sets. The segmented sulcal regions corresponding to the right and left central, superior frontal, cingulate, and parieto-occipital sulci were manually labeled on each of the 105 cortical surfaces using PALS. The locations of these sulcal regions are illustrated in Figs. 13a and b and a detailed description of the labeling procedure for each of the sulcal regions is given below.

All labeling was performed by a single user (M.E.R.). The user labeled one sulcal region on all 105 brains before continuing to the next one. For example, first all left central sulcal regions were labeled, then all right central sulcal regions, etc. We found this technique made it easier for the user to consistently identify sulcal patterns across the various cortical surfaces. It took approximately 142 h to label all eight sulcal regions on the 105 brains giving an average labeling time of approximately 1 h and 20 min per brain. A substantial portion of this time was

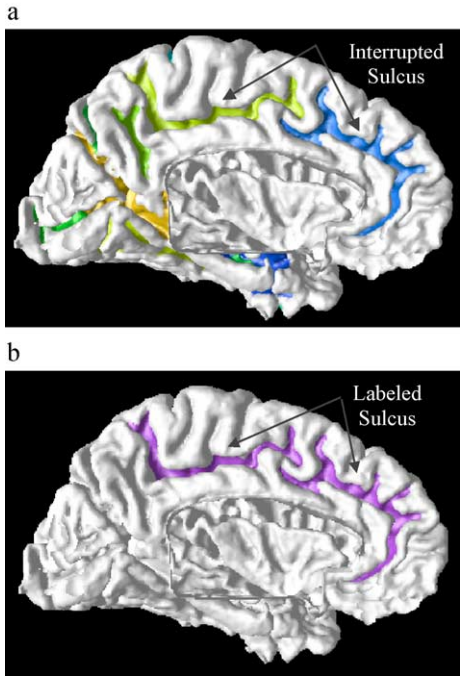

Fig. 18. This cortex has an interrupted cingulate sulcus as illustrated in a. The two regions must be grouped to label this region, as shown in b.

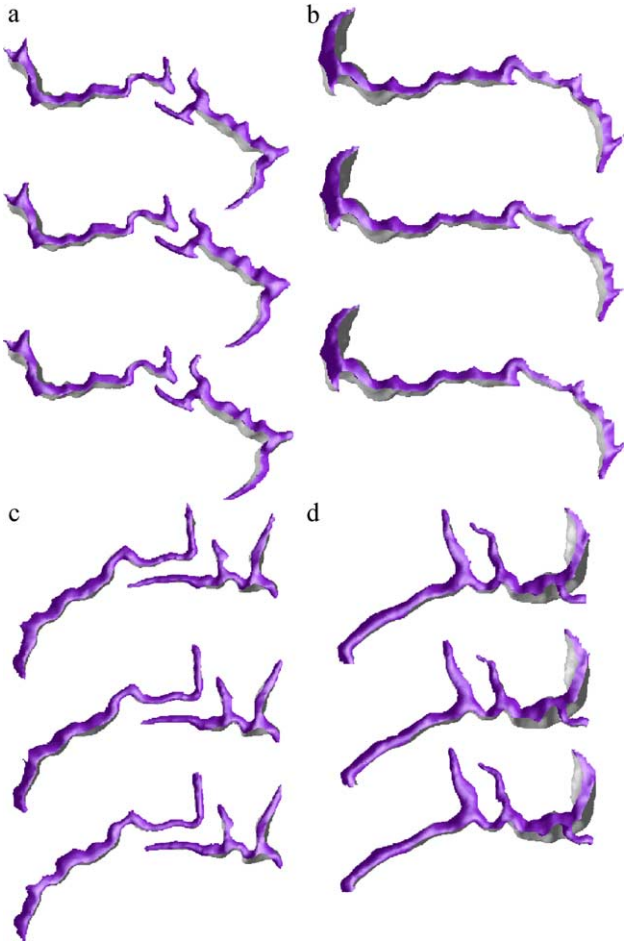

Fig. 19. The labeled left (a, b) and right (c, d) cingulate sulcal regions for the three scans of various individuals.

required for making decisions regarding the location and patterns of the sulci studied.

Labeling procedure

There were two main goals for the labeling procedure. The first was to properly label each of the sulcal regions according to anatomic convention. We used Ono et al.'s (1990) *Atlas of the Cerebral Sulci* to guide us in labeling each of the sulcal regions. In this atlas, Ono et al. examined 25 postmortem brains and compiled a detailed description of sulcal patterns, connections, and interruptions.

The second goal in the labeling procedure was to consistently label the sulcal regions across the three scans for each individual. This is very important as we are assessing the stability of these measurements for the use in longitudinal analyses of cortical changes. To ensure that even small changes can be detected, it is critical that the sulcal regions are labeled exactly the same across the multiple scans. For example, changes in gray matter volume could potentially be about the size of a small side branch of a sulcus. Therefore, in the labeling procedure, we had to ensure that a sulcal side branch was either consistently included or excluded across all three scans. For this reason, we labeled the three scans corresponding to a single subject simultaneously, but the rater was blinded as to the year of each scan.

During the labeling procedure, the user documented the number of times each of the operations provided by the PALS interface was used for each of the labeled regions. This information is provided in Table 1 for each labeled sulcal region. The default merging level is the highest merging level in which the height threshold is set to 1 cm and the area threshold is set to 3 cm^2 (see "Background"). We refer to this table more extensively in the following paragraphs as we describe the specific labeling procedure for each sulcal region.

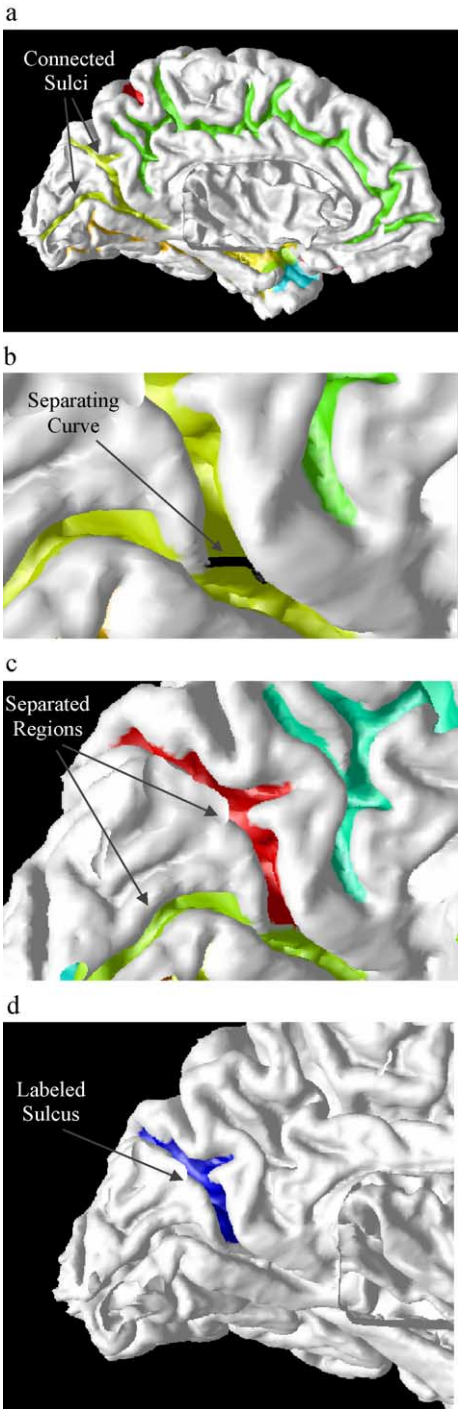

Fig. 20. At the default merging level, the parieto-occipital and calcarine sulcal regions are connected (a). The catchment basin separation operation is used to separate these regions with the separating curve shown in b and the separated regions shown in c. The final labeled region is illustrated in d.

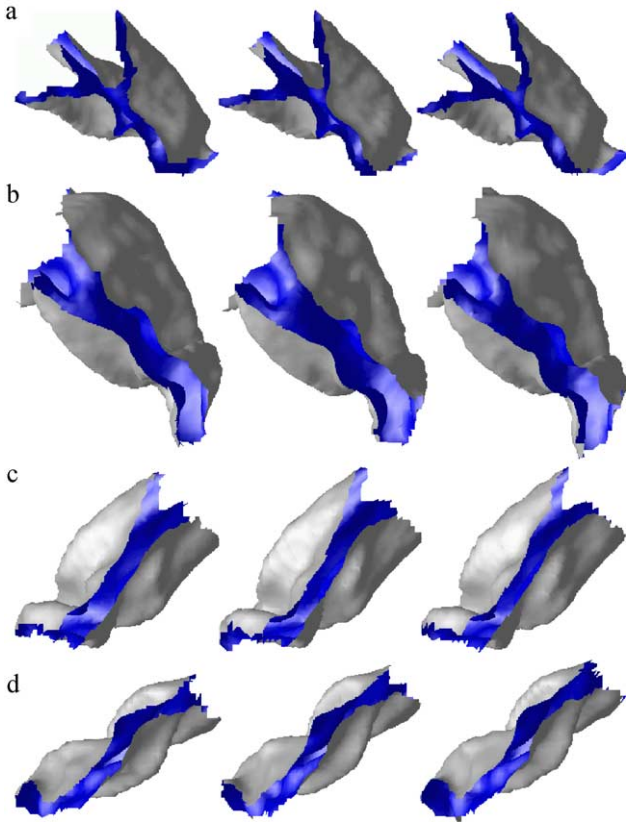

Fig. 21. The labeled left (a, b) and right (c, d) parieto-occipital sulcal regions for the three scans of various individuals.

We now give a detailed description of the labeling procedure for the four sulcal regions included in the study.

Central. The central sulcus is located on the lateral surface of the cortex as illustrated in Fig. 13a. The central sulcus is typically a continuous sulcus (i.e., no interruptions); in fact, in Ono et al.'s (1990) analysis, the central sulcus was continuous over 90% of the time.

This was the most straightforward of the four sulcal regions to label as it has the least variability in its pattern and was therefore the easiest to identify. As seen in Table 1, the vast majority of central sulcal regions were labeled either as a single piece or as multiple pieces at the default level of merging, which requires simply clicking on the region or regions with the mouse. On occasion, we did need to decrease the merging level to separate the central sulcal region from another sulcal region. For example, as shown in Fig. 14a, there is a connection between the central sulcal region and a branch over the postcentral gyrus. To remove this connection, we decreased the merging level as shown in Fig. 14b. In this figure, we see the erroneous branch is disconnected allowing the user to now label the appropriate region, as illustrated in Fig. 14c.

Table 2
Correlation values for the area measurements

Sulcus	Year 1 vs. Year 3	Year 1 vs. Year 5	Year 3 vs. Year 5
Ce_l	0.975	0.972	0.984
Ce_r	0.989	0.990	0.990
SF_l	0.982	0.975	0.983
SF_r	0.964	0.984	0.963
$Cing_l$	0.976	0.968	0.974
$Cing_r$	0.955	0.967	0.952
PO_l	0.981	0.983	0.985
PO_r	0.967	0.987	0.982

(N = 33, 34, or 35).

Table 3
Correlation values for the gray matter volume measurements

Sulcus	Year 1 vs. Year 3	Year 1 vs. Year 5	Year 3 vs. Year 5
Ce_l	0.912	0.911	0.902
Ce_r	0.892	0.894	0.879
SF_l	0.986	0.983	0.981
SF_r	0.968	0.980	0.974
$Cing_l$	0.968	0.979	0.980
$Cing_r$	0.955	0.976	0.962
PO_l	0.933	0.946	0.966
PO_r	0.864	0.950	0.931

(N = 33, 34, or 35).

The labeled left and right central sulcal regions for the three scans of various individuals are illustrated in Fig. 15. These images illustrate that the central sulcal regions are segmented and labeled in a consistent fashion across the three scans.

Superior frontal. The superior frontal sulcus is located on the lateral surface of the cortex as illustrated in Fig. 13a. The pattern of the superior frontal sulcus is quite variable. For example, in Ono et al.'s atlas, the right superior frontal sulcus was found to be continuous 40% of the time, interrupted into two segments 52% of the time, and interrupted into three segments 8% of the time. For the left superior frontal sulcus, Ono et al. found it to be continuous 32% of the time, interrupted into two segments 36% of the time, interrupted into three segments 28% of the time, and interrupted into four segments 4% of the time. In addition, the superior frontal sulcus is typically connected to the precentral sulcus. In fact, Ono et al. found this connection on the left 100% of the time and on the right 92% of the time.

Consistent with Ono et al.'s findings, we also found a connection between the superior frontal and precentral sulci in a large majority of cortical surfaces. We found that it was easiest to separate the two sulcal regions at the default level of merging and then label the superior frontal region as one or more pieces at this level. This is shown in Table 1 where most of the superior frontal sulcal regions are labeled at the default merging level, but the catchment basin separation is used a large number of times. We note that the catchment basin separation was used more than once on several superior frontal sulcal regions if it was connected to both the precentral and another sulcus. The most common connection, however, was to the precentral. An example of these connected sulcal regions is shown in Fig. 16a at the default merging level. The catchment basin separation operation was used to separate these regions with the separating curve shown in Fig. 16b and the separated regions shown in Fig. 16c. The final labeled region is illustrated in Fig. 16d.

The labeled left and right superior frontal sulcal regions for the three scans of various individuals are illustrated in Fig. 17. These images demonstrate the large variability in the patterns of the superior frontal sulcal regions; however, they are still segmented and labeled consistently across the three scans.

Cingulate. The cingulate sulcus is located on the medial surface of the cortex as illustrated in Fig. 13b. In Ono et al.'s atlas, the

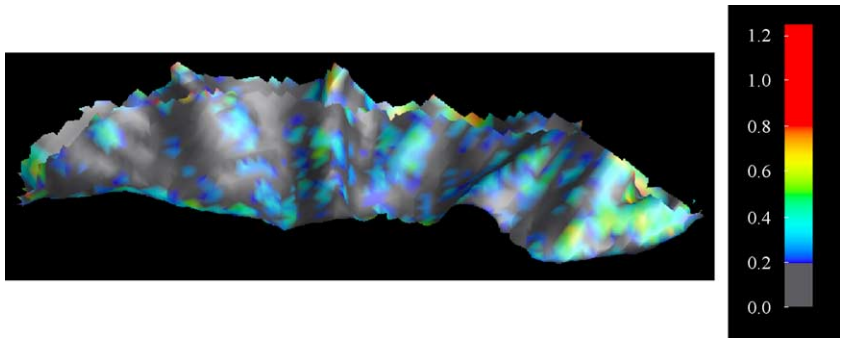

Fig. 22. The distances (in mm) mapped onto the left central sulcus of one subject.

authors found that both the left and right cingulate sulci were continuous just over 50% of the time and were otherwise interrupted into two or three segments.

During our labeling procedure, we also found the cingulate sulcal region occurred as either one, two, or three pieces. Referring to Table 1, we see the most common operations performed were labeling as one piece at the default merging level, grouping sulcal regions at the default merging level, grouping at the default and then erasing one or more pieces at a lower level, and grouping pieces at a lower level. For example, in Fig. 18a, we see the cingulate sulcus consists of two pieces at the default merging level. These can easily be grouped using PALS to label this sulcal region as illustrated in Fig. 18b.

The labeled left and right cingulate sulcal regions for the three scans of various individuals are illustrated in Fig. 19. These images show examples of both continuous as well as interrupted cingulate sulci. In addition, these images demonstrate a consistent segmentation and labeling of these regions.

Parieto-occipital. The parieto-occipital sulcus is located on the medial surface of the cortex as illustrated in Fig. 13b. The parieto-occipital sulcus forms a connection with the calcarine sulcus; in fact, Ono et al. found this connection 100% of the time in their study.

We also found a connection between the parieto-occipital and calcarine sulci in our data sets. On occasion, it was possible to separate these sulcal regions by decreasing the merging level; however, in most cases, we found it easiest to separate these sulci using the catchment basin separation operation at the default merging level and then label the parieto-occipital as one or more pieces. This is shown in Table 1 where most of the parieto-occipital sulcal regions are labeled at the default merging level, but the catchment basin separation is used a large number of times. An example of connected parieto-occipital and calcarine sulci is shown in Fig. 20a at the default merging level. The catchment basin separation operation is used to separate these regions with the separating curve shown in Fig. 20b and the separated regions shown in Fig. 20c. The final labeled region is illustrated in Fig. 20d.

The labeled left and right parieto-occipital sulcal regions for the three scans of various individuals are illustrated in Fig. 21, again demonstrating a consistent segmentation and labeling of these regions.

Stability analysis results

During the labeling procedure, we found the surface model generated for one data set at one time point appeared noisy and inaccurate and was therefore dropped from the analysis. In addition, of the 832 sulcal regions labeled, 3 were not segmented correctly and were also dropped from the analysis.

The surface area and gray matter volume were computed for all properly segmented sulcal regions. Thus, for each sulcal region, we had either 33, 34, or 35 sets of repeated measurements. We assess the stability of these measures by computing Pearson correlation coefficients between the various year pairs. For each geometric feature, we report the correlation coefficients on the measurements made between year 1 and year 3, year 1 and year 5, and year 3 and year 5. The correlation values for the surface areas are reported in Table 2. The correlations are all very high, ranging from 0.952 to 0.990. The correlation values for the gray matter volume measurements are reported in Table 3. The correlations are all above 0.86 and are mostly above 0.90. The correlations for the gray matter volume measurements are somewhat lower than those for the surface area measurements. A possible explanation is that the gray matter volume is computed using both cortical thickness as well as surface area and therefore has an additional source of error.

Table 4
Distance measures (in mm) from the sulcal region obtained from scan 2 to the sulcal region obtained from scan 1

Sulcus	Subject 1		Subject 2		Subject 3	
	Mean	SD	Mean	SD	Mean	SD
Ce_l	0.22	0.19	0.19	0.16	0.21	0.19
Ce_r	0.22	0.17	0.16	0.17	0.21	0.19
SF_l	0.19	0.16	0.17	0.15	0.20	0.19
SF_r	0.21	0.17	0.16	0.15	0.18	0.17
$Cing_l$	0.26	0.30	0.20	0.24	0.22	0.32
$Cing_r$	0.20	0.18	0.17	0.17	0.18	0.20
PO_l	0.15	0.13	0.17	0.17	0.15	0.17
PO_r	0.16	0.17	0.18	0.22	0.16	0.18

Table 5
Area measurements for the repeatability analysis

Sulcus	Subject 1		Subject 2		Subject 3	
	Scan 1	Scan 2	Scan 1	Scan 2	Scan 1	Scan 2
Ce_l	2446	2387	2459	2479	2828	2768
Ce_r	2747	2725	2559	2527	3006	2983
SF_l	4054	4010	3418	3472	2904	2920
SF_r	3702	3523	1705	1743	1524	1518
$Cing_l$	1616	1614	2307	2400	2926	3020
$Cing_r$	1756	1824	2266	2218	2505	2510
PO_l	1189	1203	1579	1568	1336	1343
PO_r	1661	1665	1650	1702	1597	1576

Values are reported in mm^2.

Table 6
Absolute and percent differences for the area measurements

	Ce_l		Ce_r		SF_l		SF_r		$Cing_l$		$Cing_r$		PO_l		PO_r	
	Absolute	%	Absolute	%	Absolute	%	Absolute	%	Absolute	%	Absolute	%	Absolute	%	Absolute	%
Subject 1	59	2.41	22	0.80	44	1.09	179	4.84	2	0.12	68	3.87	14	1.18	4	0.24
Subject 2	20	0.81	32	1.25	54	1.58	38	2.23	93	4.03	48	2.12	11	0.70	52	3.15
Subject 3	60	2.12	23	0.77	16	0.55	6	0.39	94	3.21	5	0.20	7	0.52	21	1.31
Mean	46.33	1.78	25.67	0.94	38.00	1.07	74.33	2.49	63.00	2.45	40.33	2.06	10.67	0.80	25.67	1.57
SD	22.81	0.85	5.51	0.27	19.70	0.52	92.05	2.24	52.83	2.06	32.19	1.84	3.51	0.34	24.34	1.47

Ce = central, SF = superior frontal, Cing = cingulate, PO = parieto-occipital; l = left, r = right.

Table 7
Gray matter volume measurements for the repeatability analysis

Sulcus	Subject 1		Subject 2		Subject 3	
	Scan 1	Scan 2	Scan 1	Scan 2	Scan 1	Scan 2
Ce_l	4123	3659	3751	3676	4337	4495
Ce_r	4497	3889	3323	3353	4459	4706
SF_l	9532	9600	8715	8855	6921	7105
SF_r	7319	7468	4084	4103	3458	3424
$Cing_l$	3751	3790	5849	6159	7246	7513
$Cing_r$	4040	4144	5596	5512	6205	6428
PO_l	2416	2345	3465	3387	2884	2914
PO_r	3746	3783	3942	4004	3770	3676

Values are reported in mm^3.

Repeatability analysis

In the repeatability analysis, three individuals were each scanned twice. Each of the repeated scans was performed within a 30-min time interval during which the subject was repositioned in the scanner. For each of the MR data sets acquired, the cortical surfaces, spherical maps, and hierarchical sulcal segmentations were computed. Eight sulcal regions on each cortical surface were again labeled by a single user (M.E.R.) using PALS. The regions selected for labeling were the same as those in the stability analysis—the regions of cortex corresponding to the left and right central, superior frontal, cingulate, and parieto-occipital sulci. The labeling procedure was analogous to that described in the previous section.

It took approximately 1 h and 15 min per brain to label the eight sulcal regions. Of the 48 total sulci labeled, 16 were labeled as a single region at the highest level of merging, 18 were labeled by grouping two or more regions at the highest level of merging, and 14 were labeled by grouping two or more catchment regions at a decreased merging level. In addition, a total of 17 catchment basin separations were required. Of these, 10 were used to separate the superior frontal sulcus from the precentral sulcus, 5 were used to separate the parieto-occipital sulcus from the calcarine sulcus, and 2 were used to separate the central sulcal from the medial frontal sulcus.

We use two approaches to assess the repeatability of the techniques. The first approach aims to quantify the similarity of the sulcal regions segmented from the two scans. The second approach quantifies the repeatability of the area and gray matter volume measurements for each sulcal region between the two scans.

Distance between sulcal regions

In the first approach for assessing repeatability, we measure the distance between the sulcal regions obtained for the two scans. This distance is computed separately for each sulcal region as follows. First, the sulcal region segmented from scan 2 was rigidly registered to scan 1 using a modified iterative closest points (ICP) algorithm (Tosun et al., 2003). The ICP modification is that the corresponding closest point to a given surface vertex is computed as its projection onto the other surface, and this is done symmetrically for all vertices of both surfaces. The entire cortical surfaces are first globally registered to give an initial overall alignment followed by a local registration of the individual sulcal regions. Next, for each point on the sulcal region from scan 2, we compute the closest distance to the sulcal region from scan 1. This provides a distance measure for each vertex on the sulcal region from scan 2. An example of the result of

this operation is illustrated on the left central sulcus of one subject in Fig. 22 where each distance is represented by the color indicated in the color bar. All areas colored in gray have errors in the range from 0 to 0.2 mm and all errors above 0.8 mm are colored in red. This figure illustrates that the errors are, for the most part, spread across the entire region; however, the points with the largest errors tend to occur on the boundaries. This pattern was also observed in other sulcal regions indicating the largest registration errors are occurring along the region boundaries. In Table 4, the mean and standard deviation of the distances computed for each sulcal region of the three subjects are given in millimeters. The mean distance between the same sulcal regions segmented from the two scans ranges from 0.15 to 0.26 mm.

Repeatability of area and volume measurements

The second approach for quantifying repeatability focuses on the repeatability of the surface area and gray matter volume measurements as opposed to the distance between the sulcal regions. In this procedure, first the surface area and gray matter volume measurements were computed on the selected regions for both scans of the three subjects. We assess the repeatability of the measurements by comparing the values computed for each sulcal region of an image pair. In general, we consider percentage differences less than 5% to be good, but this depends on the magnitude of the measurement. Reporting errors as percentage differences can be misleading as smaller measurements will have larger errors. For this reason, we also include the absolute differences.

The surface areas measured for the three repeated scans are given in Table 5 with the absolute and percentage differences reported in Table 6. All percentage differences are less than 5%. The gray matter volumes are given in Table 7 with the absolute and percentage differences reported in Table 8. In 20 of the 24 sulcal regions, the percentage differences are less than 5%.

Discussion and conclusions

In this paper, we have described and validated an efficient procedure for assigning anatomical labels to sulcal regions. The procedure has two important features. The first is a graph structure that provides the ability to move between various merging levels of the sulcal segmentation allowing the user to quickly assess the most appropriate level for labeling each sulcal region. The second feature is the ability to separate either an individual catchment basin or a region of merged catchment basins with a user-specified curve. When combined together, these two features augment our original sulcal segmentation to provide a complete system for segmenting and labeling sulcal regions of a brain cortex.

We have also conducted several reliability experiments aimed to assess both the long-term stability as well as the short-term repeatability of these techniques. In the stability analysis, we concluded that both the area and volume measurements were stable over a 4-year time span. In the repeatability analysis, we found that both the sulcal segmentation itself as well as the area and volume measurements were highly repeatable.

One limitation of the described work is that the labeling was performed by only a single individual and thus there is no inter-rater reliability analysis. The user did, however, label each sulcal region one at a time across all brains, which we believe improved the consistency of identifying the various sulcal patterns.

Table 8
Absolute and percent differences for the gray matter volume measurements

	Ce_l		Ce_r		SF_l		SF_r		$Cing_l$		$Cing_r$		PO_l		PO_r	
	Absolute	%	Absolute	%	Absolute	%	Absolute	%	Absolute	%	Absolute	%	Absolute	%	Absolute	%
Subject 1	464	11.25	608	13.52	68	0.71	149	2.04	39	1.04	104	2.57	71	2.94	37	0.99
Subject 2	75	2.00	30	0.90	140	1.61	19	0.47	310	5.30	84	1.50	78	2.25	62	1.57
Subject 3	158	3.64	247	5.54	184	2.66	34	0.98	267	3.68	223	3.59	30	1.04	94	2.49
Mean	232.33	5.63	295.00	6.65	130.67	1.66	67.33	1.16	205.33	3.34	137.00	2.55	59.67	2.08	64.33	1.68
SD	204.88	4.94	291.97	6.38	58.56	0.98	71.12	0.80	145.64	2.15	75.15	1.05	25.93	0.96	28.57	0.76

Ce = central, SF = superior frontal, Cing = cingulate, PO = parieto-occipital; l = left, r = right.

This interface has also been used in other works (Behnke et al., 2003; Tosun et al., 2003) to label sulcal regions that are subsequently used as training sets in automatic labeling schemes. These labeling schemes have shown promising results and could be used to improve the methodologies proposed in this paper by providing an initial labeling of the sulcal regions. The automatically generated labels would then be manually verified (and corrected, if necessary) using PALS. This could potentially provide a significant reduction in the time required for manual interaction and therefore increase the number of subjects feasible for a study.

In summary, we have described a procedure for efficiently assigning anatomical labels to sulcal regions and demonstrated the techniques are both stable and repeatable. In future work, we intend to use these techniques in an aging study to assess both cross-sectional differences as well as longitudinal changes in sulcal shape associated with age. In addition, we will investigate whether these measurements provide complementary information to enhance early detection of cognitive impairment and Alzheimer's disease.

Acknowledgments

The authors would like to thank Dr. Dzung Pham for assistance with the MR data and Dr. Michael Kraut for his expertise regarding this work.

References

Bartesaghi, A., Sapiro, G., 2001. A system for the generation of curves on 3D brain images. Hum. Brain. Mapp. 14 (1), 1–15.

Behnke, K.J., Rettmann, M.E., Pham, D.L., Shen, D., Davatzikos, C., Resnick, S.M., Prince, J.L., 2003. Automatic classification of sulcal regions of the human brain cortex using pattern recognition. Proc. SPIE. Med. Imag. 5032, 1499–1510.

Cachia, A., Mangin, J.F., Riviere, D., Papadopoulos-Orfanos, D., Kherif, F., Bloch, I., Regis, J., 2003a. A generic framework for parcellation of the cortical surface into gyri using geodesic Voronoi diagrams. Med. Image. Anal. 7 (4), 403–416.

Cachia, A., Mangin, J.F., Riviere, D., Kherif, F., Boddaert, N., Andrade, A., Papadopoulos-Orfanos, D., Poline, J.B., Bloch, I., Zilbovicius, M., Sonigo, P., Brunelle, F., Regis, J., 2003b. A primal sketch of the cortex mean curvature: a morphogenesis based approach to study the variability of the folding patterns. IEEE. Trans. Med. Imag. 22 (6), 754–765.

Cannon, T.D., Thompson, PM., van Erp, T.G., Toga, A.W., Poutanen, V.P., Huttunen, M., Lonnqvist, J., Standerskjold-Nordenstam, C.G., Narr, K.L., Khaledy, M., Zoumalan, C.I., Dail, R., Kaprio, J., 2002. Cortex mapping reveals regionally specific patterns of genetic and disease-specific gray-matter deficits in twins discordant for schizophrenia. Proc. Natl. Acad. Sci. 99 (5), 3228–3233.

Caviness Jr., V.S., Meyer, J., Makris, N., Kennedy, D.N., 1996. MRI-based topographic parcellation of human neocortex: an anatomically specified method with estimate of reliability. J. Cogn. Neurosci. 8 (6), 566–587.

Chan, D., Janssen, J.C., Whitwell, J.L., Watt, H.C., Jenkins, R., Frost, C., Rossor, M.N., Fox, N.C., 2003. Change in rates of cerebral atrophy over time in early-onset Alzheimer's disease: longitudinal MRI study. Lancet 362 (9390), 1121–1122.

Crespo-Facorro, B., Kim, J., Andreasen, N.C., O'Leary, D.S., Wiser, A.K., Bailey, J.M., Harris, G., Magnotta, V.A., 1999. Human frontal cortex: an MRI-based parcellation method. NeuroImage 10 (5), 500–519 (April).

Davatzikos, C., Bryan, R.N., 2002. Morphometric analysis of cortical sulci using parametric ribbons: a study of the central sulcus. J. Comput. Assist. Tomogr. 26 (2), 298–307.

Fischl, B., Dale, A., 2000. Measuring the thickness of the human cerebral cortex from magnetic resonance images. Proc. Natl. Acad. Sci. 97 (20), 11050–11055.

Fischl, B., van der Kouwe, A., Destrieux, C., Halgren, E., Ségonne, F., Salat, D.H., Busa, E., Seidman, L.J., Goldstein, J., Kennedy, D., Caviness, V., Makris, N., Rosen, B., Dale, A.M., 2004. Automatically parcellating the human cerebral cortex. Cereb. Cortex. 14 (1), 11–22.

Good, C.D., Johnsrude, I.S., Ashburner, J., Henson, R.N.A., Friston, K.J., Frackowiak, R.S.J., 2001. A voxel-based morphometric study of ageing in 465 normal adult human brains. NeuroImage 14 (1), 21–36.

Grenander, U., Miller, M.I., 1998. Computational anatomy: an emerging discipline. Q. Appl. Math. 56, 617–694.

Han, X., Xu, C., Braga-Neto, U., Prince, J.L., 2001a. Graph-based topology correction for brain cortex segmentation. Proceedings of the XVIIth International Conference on Information Processing in Medical Imaging (IPMI'01), Lecture Notes in Computer Science, vol. 2082, pp. 395–401.

Han, X., Xu, C., Rettmann, M.E., Prince, J.L., 2001b. Automatic segmentation editing for cortical surface reconstruction. Proc. SPIE. Med. Imag. 4322, 194–203.

Han, X., Xu, C., Prince, J.L., 2001c. Cortical surface reconstruction using a topology preserving geometric deformable model. The Fifth IEEE Workshop on Mathematical Methods in Biomedical Image Analysis (MMBIA), pp. 213–220.

Jouandet, M.L., Tramo, M.J., Herron, D.M., Hermann, A., Loftus, W.C., Bazell, J., Gazzaniga, M.S., 1989. Brainprints: computer-generated two-dimensional maps of the human cerebral cortex in vivo. J. Cogn. Neurosci. 1 (1), 88–117.

Kikinis, R., Shenton, M.E., Gerig, G., Hokama, H., Haimson, J., O'Donnell, B.F., Wible, C.G., McCarley, R.W., Jolesz, F.A., 1994. Temporal lobe sulco-gyral pattern anomalies in schizophrenia: an in vivo MR three-dimensional surface rendering study. Neurosci. Lett. 182 (1), 7–12.

Kim, J., Crespo-Facorro, B., Andreasen, N.C., O'Leary, D.S., Zhang, B., Harris, G., Magnotta, V.A., 2000. An MRI-based parcellation method for the temporal lobe. NeuroImage 11 (4), 271–288.

Kimmel, R., Sethian, J.A., 1998. Computing geodesic paths on manifolds. Proc. Natl. Acad. Sci. 95 (15), 8431–8435.

Kuperberg, G.R., Broome, M.R., McGuire, P.K., David, A.S., Eddy, M., Ozawa, F., Goff, D., West, W.C., Williams, S.C., van der Kouwe, A.J., Salat, D.H., Dale, A.M., Fischl, B., 2003. Regionally localized thinning of the cerebral cortex in schizophrenia. Arch. Gen. Psychiatry 60 (9), 878–888.

Le Goualher, G., Procyk, E., Collins, D.L., Venugopal, R., Barillot, C., Evans, A.C., 1999. Automated extraction and variability analysis of sulcal neuroanatomy. IEEE. Trans. Med. Imag. 18 (3), 206–217.

Leonard, C.M., Williams, C.A., Nicholls, R.D., Agee, O.F., Voeller, K.K.S., Honeyman, J.C., Staab, E.V., 1993. Angelman and Prader–Willi Syndrome: a magnetic resonance imaging study of differences in cerebral structure. Am. J. Med. Genet. 46 (1), 26–33.

Levitt, J.G., Blanton, R.E., Smalley, S., Thompson, P.M., Guthrie, D., McCracken, J.T., Sadoun, T., Heinichen, L., Toga, A.W., 2003. Cortical sulcal maps in autism. Cereb. Cortex. 13 (7), 728–735.

Lohmann, G., von Cramon, D.Y., 2000. Automatic labelling of the human cortical surface using sulcal basins. Med. Image. Anal. 4 (3), 179–188.

Magnotta, V.A., Andreasen, N.C., Schultz, S.K., Harris, G., Cizadlo, T., Heckel, D., Nopoulos, P., Flaum, M., 1999. Quantitative in vivo measurement of gyrification in the human brain: changes associated with aging. Cereb. Cortex. 9 (2), 151–160.

Manceaux-Demiau, A., Bryan, R.N., Davatzikos, C., 1998. A probabilistic ribbon model for shape analysis of the cerebral sulci: application to the central sulcus. J. Comput. Assist. Tomogr. 22 (6), 962–971.

Mangin, J.F., Regis, J., Bloch, I., Frouin, V., Samson, Y., Lopez-Krahe, J., 1995a. A Markovian random field based random graph modelling the human cortical topography. First International Conference on Computer

Vision, Virtual Reality and Robotics in Medicine, Lecture Notes in Computer Science, vol. 905, pp. 177–183.
Mangin, J.F., Frouin, V., Bloch, I., Regis, J., Lopez-Krahe, J., 1995b. From 3D magnetic resonance images to structural representations of the cortex topography using topology preserving deformations. J. Math. Imaging. Vis. 5, 297–318.
Mangin, J.F., Riviere, D., Coulon, O., Poupon, C., Cachia, A., Cointepas, Y., Poline, J.B., Le Bihan, D., Regis, J., Papadopoulos-Orfanos, D., 2003. Coordinate-based versus structural approaches to brain image analysis. Artif. Intell. Med. 30 (2), 177–197.
Meyer, F., Beucher, S., 1990. Morphological segmentation. J. Vis. Commun. Image. Represent. 1 (1), 21–46.
Miller, M.I., Massie, A.B., Ratnanather, J.T., Botteron, K.N., Csernansky, J.G., 2000. Bayesian construction of geometrically based cortical thickness metrics. NeuroImage 12 (6), 676–687.
Miller, M.I., Hosakere, M., Barker, A.R., Priebe, C.E., Lee, N., Ratanather, J.T., Wang, L., Gado, M., Morris, J.C., Csernansky, J.G., 2003. Labeled cortical mantle distance maps of the cingulate quantify differences between dementia of the Alzheimer type and healthy aging. Proc. Natl. Acad. Sci. 100 (25), 15172–15177.
Molko, N., Cachia, A., Riviere, D., Mangin, J.F., Bruandet, M., Le Bihan, D., Cohen, L., Dehaene, S., 2003. Functional and structural alterations of the intraparietal sulcus in a developmental dyscalculia of genetic origin. Neuron 40 (4), 847–858.
Murphy, D.G.M., DeCarli, C., McIntosh, A.R., Daly, E., Mentis, M.J., Pietrini, P., Szczepanik, J., Schapiro, M.B., Grady, C.L., Horwitz, B., Rapoport, S.I., 1996. Sex differences in human brain morphometry and metabolism: an in vivo quantitative magnetic resonance imaging and positron emission tomography study on the effect of aging. Arch. Gen. Psychiatry. 53 (7), 585–594.
Ono, M., Kubick, S., Abernathey, C.D., 1990. Atlas of the Cerebral Sulci. Thieme, New York.
Pfefferbaum, A., Mathalon, D.H., Sullivan, E.V., Rawles, J.M., Zipursky, R.B., Lim, K.O., 1994. A quantitative magnetic resonance imaging study of changes in brain morphology from infancy to late adulthood. Arch. Neurol. 51 (9), 874–887.
Rademacher, J., Galaburda, A.M., Kennedy, D.N., Filipek, P.A., Caviness Jr., V.S., 1992. Human cerebral cortex: localization, parcellation, and morphometry with magnetic resonance imaging. J. Cogn. Neurosci. 4 (4), 352–374.
Ratnanather, J.T., Botteron, K.N., Nishino, T., Massie, A.B., Lal, R.M., Patel, S.G., Peddi, S., Todd, R.D., Miller, M.I., 2001. Validating cortical surface analysis of medial prefrontal cortex. NeuroImage 14 (5), 1058–1069.
Ratnanather, J.T., Barta, P.E., Honeycut, N.A., Lee, N., Morris, H.M., Dziorny, A.C., Hurdal, M.K., Pearlson, G.D., Miller, M.I., 2003. Dynamic programming generation of boundaries of local coordinated submanifolds in the neocortex: application to the planum temporale. NeuroImage 20 (1), 359–377.
Raz, N., Torres, I.J., Briggs, S.D., Spencer, W.D., Thornton, A.E., Loken, W.J., Gunning, F.M., McQuain, J.D., Driesen, N.R., Acker, J.D., 1995. Selective neuroanatomic abnormalities in Down's syndrome and their cognitive correlates: evidence from MRI morphometry. Neurology 45 (2), 356–366.
Raz, N., Gunning, F.M., Head, D., Dupuis, J.H., McQuain, J., Briggs, S.D., Loken, W.J., Thornton, A.E., Acker, J.D., 1997. Selective aging of the human cerebral cortex observed in vivo: differential vulnerability of the prefrontal gray matter. Cereb. Cortex. 7 (3), 268–282.
Resnick, S.M., Goldszal, A.F., Davatzikos, C., Golski, S., Kraut, M.A., Metter, E.J., Bryan, R.N., Zonderman, A.B., 2000. One-year age changes in MRI brain volumes in older adults. Cereb. Cortex. 10 (5), 464–472.
Resnick, S.M., Pham, D.L., Kraut, M.A., Zonderman, A.B., Davatzikos, C., 2003. Longitudinal magnetic resonance imaging studies of older adults: a shrinking brain. J. Neurosci. 23 (8), 3295–3301.
Rettmann, M.E., Tao, X., Prince, J.L., 2002a. Assisted labeling techniques for the human brain cortex. Proc. SPIE. Med. Imag. 4684, 179–190.
Rettmann, M.E., Han, X., Xu, C., Prince, J.L., 2002b. Automated sulcal segmentation using watersheds on the cortical surface. NeuroImage 15 (2), 329–344.
Rosas, H.D., Liu, A.K., Hersch, S., Glessner, M., Ferrante, R.J., Salat, D.H., van der Kouwe, A., Jenkins, B.G., Dale, A.M., Fischl, B., 2002. Regional and progressive thinning of the cortical ribbon in Huntington's disease. Neurology 58 (5), 695–701.
Royackkers, N., Desvignes, M., Fawal, H., Revenu, M., 1999. Detection and statistical analysis of human cortical sulci. NeuroImage 10 (6), 625–641.
Sailer, M., Fischl, B., Salat, D., Tempelmann, C., Schonfeld, M.A., Busa, E., Bodammer, N., Heinze, H.J., Dale, A., 2003. Focal thinning of the cerebral cortex in multiple sclerosis. Brain 126 (8), 1734–1744.
Salat, D.H., Buckner, R.L., Snyder, A.Z., Greve, D.N., Desikan, R.S.R., Busa, E., Morris, J.C., Dale, A.M., Fischl, B., 2004. Thinning of the cerebral cortex in aging. Cereb. Cortex. 14 (7), 721–730.
Scahill, R.I., Schott, J.M., Stevens, J.M., Rossor, M.N., Fox, N.C., 2002. Mapping the evolution of regional atrophy in Alzheimer's disease: unbiased analysis of fluid-register serial MRI. Proc. Natl. Acad. Sci. 99 (7), 4703–4707.
Scahill, R.I., Frost, C., Jenkins, R., Whitwell, J.L., Rossor, M.N., Fox, N.C., 2003. A longitudinal study of brain volume changes in normal aging using serial registered magnetic resonance imaging. Arch. Neurol. 60 (7), 989–994.
Sebire, G., Goutieres, F., Tardieu, M., Landrieu, P., Aicardi, J., 1995. Extensive macrogyri or no visible gyri: distinct clinical, electro-encephalographic, and genetic features according to different imaging patterns. Neurology 45 (6), 1105–1111.
Shock, N.W., Greulich, R.C., Andres, R., Arenberg, D., Costa Jr., P.T., Lakatta, E., Tobin, J.D., 1984. Normal Human Aging: The Baltimore Longitudinal Study of Aging. US Government Printing Office, Washington, DC.
Sowell, E.R., Peterson, B.S., Thompson, P.M., Welcome, S.E., Henkenius, A.L., Toga, A.W., 2003. Mapping cortical change across the human life span. Nat. Neurosci. 6 (3), 309–315.
Sullivan, E.V., Marsh, L., Mathalon, D.H., Lima, K.O., Pfefferbaum, A., 1995. Age-related decline in MRI volumes of temporal lobe gray matter but not hippocampus. Neurobiol. Aging. 16 (6), 591–606.
Tao, X., Han, X., Rettmann, M.E., Prince, J.L., Davatzikos, C., 2001. Statistical study on cortical sulci of human brains. Proceedings of the XVIIth International Conference on Information Processing in Medical Imaging (IPMI'01), Lecture Notes in Computer Science, vol. 2082, pp. 475–487.
Thompson, P.M., Schwartz, C., Toga, A.W., 1996a. High-resolution random mesh algorithms for creating a probabilistic 3D surface atlas of the human brain. NeuroImage 3 (1), 19–34.
Thompson, P.M., Schwartz, C., Lin, R.L., Khan, A.A., Toga, A.W., 1996b. Three-dimensional statistical analysis of sulcal variability in the human brain. J. Neurosci. 16 (13), 4261–4274.
Thompson, P.M., Moussai, J., Zohoori, S., Goldkorn, A., Khan, A.A., Mega, M.S., Small, G.W., Cummings, J.L., Toga, A.W., 1998. Cortical variability and asymmetry in normal aging and Alzheimer's disease. Cereb. Cortex. 8 (6), 492–509.
Thompson, P.M., Giedd, J.N., Woods, R.P., MacDonald, D., Evans, A.C., Toga, A.W., 2000. Growth patterns in the developing brain detected by using continuum mechanical tensor maps. Nature 404 (6774), 190–193.
Thompson, P.M., Mega, M.S., Woods, R.P., Zoumalan, C.I., Lindshield, C.J., Blanton, R.E., Moussai, J., Holmes, C.J., Cummings, J.L., Toga, A.W., 2001a. Cortical change in Alzheimer's disease detected with a disease-specific population-based brain atlas. Cereb. Cortex. 11 (1), 1–16.
Thompson, P.M., Vidal, C., Giedd, J.N., Gochman, P., Blumenthal, J., Nicolson, R., Toga, A.W., Rapoport, J.L., 2001b. Mapping adolescent brain change reveals dynamic wave of accelerated gray matter loss in very early-onset schizophrenia. Proc. Natl. Acad. Sci. 98 (20), 11650–11655.
Thompson, P.M., Hayashi, K.M., de Zubicaray, G., Janke, A.L., Rose, S.E., Semple, J., Herman, D., Hong, M.S., Dittmer, S.S., Doddrell, D.M., Toga, A.W., 2003. Dynamics of gray matter loss in Alzheimer's disease. J. Neurosci. 23 (3), 994–1005.

Toga, A.W., Thompson, P.M., 2002. New approaches in brain morphometry. Am. J. Geriatr. Psychiatry. 10 (1), 13–23.

Toga, A.W., Thompson, P.M., Mega, M.S., Narr, K.L., Blanton, R.E., 2001. Probabilistic approaches for atlasing normal and disease-specific brain variability. Anat. Embryol. 204 (4), 267–282.

Tosun, D., Prince, J.L., 2001. A hemispherical map for the human brain cortex. Proc. SPIE. Med. Imag. 4322, 290–300.

Tosun, D., Rettmann, M.E., Prince, J.L., 2003. Mapping techniques for aligning sulci across multiple brains. Proceedings of Medical Image Computing and Computer-Assisted Interventions (MICCAI), Lecture Notes in Computer Science, vol. 2879, pp. 862–869.

Tzourio, N., Petit, L., Mellet, E., Orssaud, C., Crivello, F., Benali, K., Salamon, G., Mazoyer, B., 1997. Use of anatomical parcellation to catalog and study structure-function relationships in the human brain. Hum. Brain. Mapp. 5 (4), 228–232.

Vaillant, M., Davatzikos, C., 1997. Finding parametric representations of the cortical sulci using an active contour model. Med. Image. Anal. 1 (4), 295–315.

Van Essen, D.C., Drury, H.A., 1997. Structural and functional analyses of human cerebral cortex using a surface-based atlas. J. Neurosci. 17 (19), 7079–7102.

Vincent, L., Soille, P., 1991. Watersheds in digital spaces: an efficient algorithm based on emersion simulations. IEEE. Trans. Pattern. Anal. Mach. Intell. 13 (6), 583–598.

Xu, C., Pham, D.L., Rettmann, M.E., Yu, D.N., Prince, J.L., 1999. Reconstruction of the human cerebral cortex from magnetic resonance images. IEEE. Trans. Med. Imag. 18 (6), 467–480.

Xu, C., Han, X., Prince, J.L., 2000. Improving cortical surface reconstruction accuracy using an anatomically consistent gray matter representation. Proceedings of the sixth International Conference on Functional Mapping of the Human Brain, p. S581.

Zeng, X., Staib, L.H., Schultz, R.T., Tagare, H., Win, L., Duncan, J.S., 1999. A new approach to 3D sulcal ribbon finding from MR images. Proceedings of Medical Image Computing and Computer-Assisted Intervention (MICCAI), Lecture Notes in Computer Science, vol. 1679. Springer-Verlag, pp. 148–157.

Zhou, Y., Thompson, P.M., Toga, A.W., 1999. Extracting and representing the cortical sulci. IEEE. Comput. Graph. Appl. 19 (3), 49–55.